

Article

Comparative Study of the Characteristics of Lower Cambrian Marine Shale and Their Gas-Bearing Controlling Factors in the Middle and Lower Yangtze Areas, South China

Hezheng Dong ^{1,2}, Dongsheng Zhou ^{1,2,*}, Ziyang Deng ^{1,2} and Xiaowei Huang ³

¹ School of Ocean Sciences, China University of Geosciences (Beijing), Beijing 100083, China; 2111210030@email.cugb.edu.cn (H.D.); 2111210013@email.cugb.edu.cn (Z.D.)

² Key Laboratory of Polar Geology and Marine Mineral Resources, China University of Geosciences (Beijing), Beijing 100083, China

³ Institute of Energy, Peking University, Beijing 100871, China; huangxiaowei@pku.edu.cn

* Correspondence: dszhou@cugb.edu.cn

Abstract: This study comparatively analyzed the geological, geochemical, reservoir, and gas-bearing characteristics of the lower Cambrian marine shale in the Middle and Lower Yangtze regions. The main factors controlling the gas-bearing properties of the shales were identified, and the favorable and unfavorable conditions for shale gas accumulation are discussed. The results show that the organic carbon contents and thermal evolution degree of the organic matter in the lower Cambrian marine shale in the Lower Yangtze area were higher than those generally found in the Middle Yangtze area. The brittle mineral composition of the Middle Yangtze area was typically low silicon and high calcium, whereas the Lower Yangtze area was characterized by high silicon and low calcium. The development of micropores in the Lower Yangtze area was poorer than in the Middle Yangtze area, with the organic pores being particularly underdeveloped. The adsorption capacity of shale in the Lower Yangtze area was obviously higher than in the Middle Yangtze area. It was considered that the organic carbon content, thermal evolution degree, and molecular structure of kerogen were the main factors that controlled the adsorption properties of the shale. In addition, the Lower Yangtze area suffered a stronger tectonic transformation and frequent magmatic activity, and the preservation conditions were inferior to those in the Middle Yangtze area.

Keywords: lower Cambrian; Middle and Lower Yangtze; marine shale; gas content; main control factors



Citation: Dong, H.; Zhou, D.; Deng, Z.; Huang, X. Comparative Study of the Characteristics of Lower Cambrian Marine Shale and Their Gas-Bearing Controlling Factors in the Middle and Lower Yangtze Areas, South China. *Minerals* **2024**, *14*, 31.

<https://doi.org/10.3390/min14010031>

Academic Editors: Rui Yang, Zhiye Gao, Yuguang Hou and Jan Golonka

Received: 17 November 2023

Revised: 15 December 2023

Accepted: 26 December 2023

Published: 28 December 2023



Copyright: © 2023 by the authors. Licensee MDPI, Basel, Switzerland. This article is an open access article distributed under the terms and conditions of the Creative Commons Attribution (CC BY) license (<https://creativecommons.org/licenses/by/4.0/>).

1. Introduction

Shale gas refers to unconventional natural gas resources that accumulate in black shales and interbedded sandy and silty shales through adsorption, dissolution, or as free gas [1,2]. Over the past two decades, the successful examples of shale gas exploration and development in North America have set off a global shale gas revolution [3–6]. China has been carrying out extensive shale gas exploration and development work since 2009 [7,8]. In recent years, marine shale gas exploration in southern China has achieved tremendous results [9,10]. The Wufeng–Longmaxi Formation shale in the Upper Yangtze area has achieved large-scale industrial gas production [11], while the Niutitang Formation in the lower Cambrian in the south of Sichuan province has also made breakthroughs in shale gas development [12,13]. The Shuijingtuo Formation in the Yichang area in the Middle Yangtze area also shows industrial-grade shale gas potential [14]. However, exploration of the lower Cambrian marine shale gas in the Lower Yangtze area has yet to achieve a significant breakthrough [15].

Shale contains various elements, including silicon, aluminum, calcium, potassium, uranium, thorium, iron, and manganese [16,17]. The significant features of the lower Cambrian marine shales in southern China are their relatively high silicon content, the

widespread development of siliceous shales, and the high organic richness of the siliceous shales [18,19]. Silicon is an important nutrient element in seawater [20] and has three currently understood sources: hydrothermal fluids [21,22], biogenesis (for example, from silicon-secreting organisms like sponges and radiolarians) [23,24], and terrestrial input [25]. Pioneering studies, notably that of Holdaway and Clayton (1982), introduced the concept of “excess silicon”, which refers to the proportion of siliceous minerals that exceeds the usual terrigenous clastic sources [26]. Wedepohl (1971), Adachi et al. (1986), and Yamamoto (1987) proposed a technique to ascertain whether silicate minerals have a hydrothermal or biogenic origin by utilizing an Al-Fe-Mn ternary diagram [16,17,27]. Previous research on the mechanisms of organic matter enrichment in lower Cambrian shales in southern China has shown that sources of silicon or conditions for organic matter enrichment vary in different regions and sedimentary environments. Numerous studies suggested that hydrothermal processes played a significant role in the genesis of silicon and organic matter enrichment in the lower Cambrian shales in southern China [28–31]. However, some argued that hydrothermal activity made little contribution to siliceous enrichment in the intra-platform basins of the Yangtze Block [32].

The lower Cambrian siliceous shales in southern China, which are rich in quartz and susceptible to hydraulic fracturing [1,33], were identified as prime targets for shale gas exploration [9]. However, shale gas accumulation is often the result of a combination of many factors [34,35]. Mineral composition, thermal evolution, pore structure, and tectonic activity all have an important influence on the gas-bearing properties of shale, especially on the adsorbed gas content [36–41]. However, the interplay between these factors is, as yet, poorly understood, and further research is needed to investigate their combined controlling effect. Research on the mechanisms of organic matter enrichment, silicon sources, and gas-bearing properties in the Lower and Middle Yangtze regions has mainly focused on individual wells or sections, and thus, there is a lack of comprehensive regional studies [41–46]. This study aimed to combine individual-well and regional-scale comparative research based on individual-well data and regional characteristics. This approach has both theoretical and practical significance for evaluating the mechanisms of organic matter enrichment and the gas-bearing properties of shales and will be a valuable aid in the assessment of shale gas exploration potential in the Lower and Middle Yangtze shales.

In this study, the factors controlling shale gas accumulation in the lower Cambrian marine shale in the Middle and Lower Yangtze regions were compared by analyzing their organic geochemistry, reservoir characteristics, pore types, and gas-bearing characteristics. The differences and relative advantages of shale gas accumulation conditions in the two regions are discussed. The objectives of this study were (1) to enhance the understanding of the lateral variations in geochemistry, petrophysics, and shale gas storage capacity within time-equivalent stratigraphic units spanning the early Cambrian period in the Middle and Lower Yangtze regions; (2) to discuss the spatial disparities observed in these elements and their controlling factors; and (3) to establish the correlations between these disparities and the potential for shale gas resources.

2. Geological Setting

The Yangtze platform is one of the three oldest in China and is divided into three tectonic units: the Upper, Middle, and Lower Yangtze regions [47] (see Figure 1). The Upper Yangtze Platform is bounded by the Qinling–Dabie orogenic belt to the north, the Red River Fault Zone to the southwest, the Xianshuihe Fault Zone to the west, and the Cathaysia Platform to the southeast [48]. The Middle Yangtze area is located in the middle reaches of the Yangtze River, bounded by the Baojing–Cili fault in the southeast and separated from the Jiangnan–Xuefeng paleo-uplift, with the Qiyueshan fault in the northwest being separated from the rest of the structure in eastern Sichuan. The area is blocked by the Huangling paleo-uplift in the north and separated from the arc structure of Dabashan Mountain and connects with the structure of Middle Guizhou in the south.

The Lower Yangtze area lies in the lower reaches of the Yangtze River, bounded by the Tancheng–Lujiang fault zone and separated from the Qinling–Dabie orogenic belt in the west, the Sulu orogenic belt in the north, and the Wuyi orogenic belt in the south [49].

Against the background of accelerated fragmentation of the Rodinia supercontinent after the Neoproterozoic [50], the South China plate initially developed an intracontinental rift [51] and then evolved into a passive continental margin under extensional tectonic movement [52]. The stratigraphic framework of the Yangtze platform near the Ediacaran–Cambrian boundary exhibited a pattern of alternating uplifts and depressions, forming two basins and a platform [53]. A large-scale marine transgression occurred in the early Cambrian, leading to widespread marine sedimentation on the platform, and the water depth gradually increased from the NW to the SE, with the Upper Yangtze developing carbonate platforms and intrashelf basin (or lagoon) sedimentation and Middle Yangtze areas primarily developing an intrashelf basin, shallow shelf, and slope [54,55]. The Lower Yangtze area developed various sedimentation types, including carbonate platforms, deep shelves, and deep basins [56,57].

The Cambrian strata in the Yangtze regions are rich in organic-rich shale, particularly in the middle and lower strata (see Figure 2). Due to frequent sea-level fluctuations in the Yangtze platform, the multi-cyclic simultaneous development of calcareous shale, marl, calcareous mudstone, siliceous rock, and limestone occurred (see Figure 2). These rock layers effectively prevented vertical migration and loss of hydrocarbons, forming an effective seal [19,45,58,59]. The lower Cambrian marine shales in the Yangtze Platform therefore have favorable preliminary conditions for shale gas accumulation. This study focused on the lower Cambrian marine shale research in the Middle and Lower Yangtze regions. Due to the different sedimentary and tectonic evolution settings in the two regions, there are certain differences in the shales, and these differences significantly affect shale gas enrichment and subsequent exploration and development in the two regions.

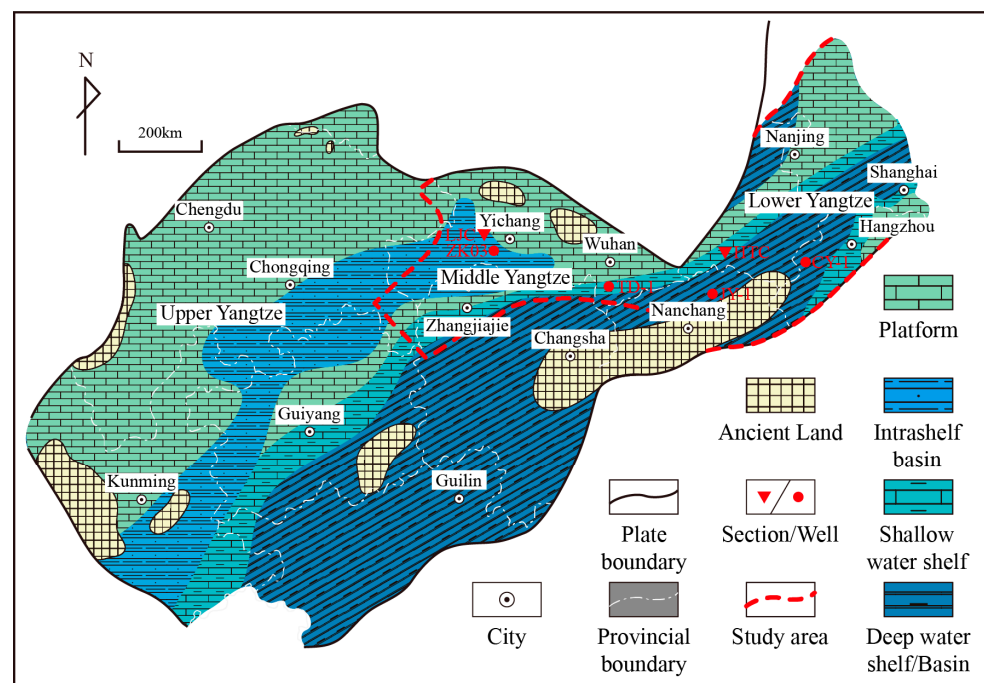


Figure 1. The location of the study area and the lithofacies paleogeography of the Yangtze Block during the early Cambrian (~530 Ma), modified from references [56,57]. The lower Cambrian organic-rich marine shale has been primarily developed in intrashelf basins, shelves, and basins.

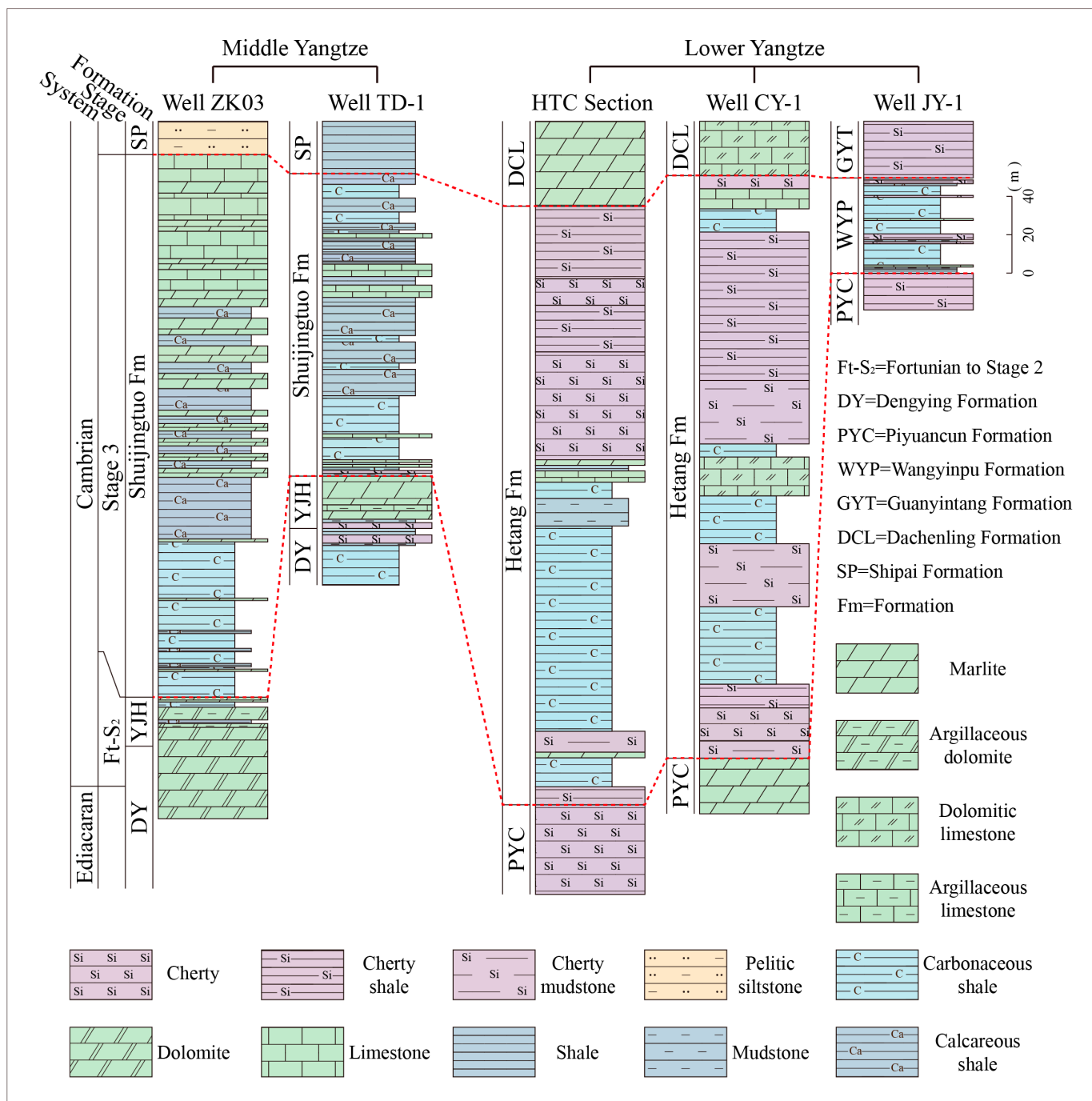


Figure 2. Correlation of the stratigraphic column of the lower Cambrian in different parts of the Middle and Lower Yangtze areas. Wells ZK03, TD-1, CY-1, and JY-1 were modified from references [19,40,45,59], respectively. The lower Cambrian organic-rich marine shale is mostly found in the middle and lower parts of the Shuijingtuo Formation and the Hetang Formation (known as the Wangyinpu Formation in northwest Jiangxi). These are coeval deposits. In the Middle Yangtze area, the Shuijingtuo Formation contains higher proportions of calcareous and argillaceous intercalations. In the Lower Yangtze area, siliceous rocks and siliceous shales have developed in the Hetang Formation.

3. Materials and Methods

3.1. Samples

Fresh outcrop samples of lower Cambrian marine shale were collected in the Middle and Lower Yangtze regions, including 8 samples from the Niutitang Formation in the northwest of the Middle Yangtze area, 18 samples from the Shuijingtuo Formation in western Hubei Province, and 7 samples from the Shuijingtuo Formation in eastern Hubei province. Furthermore, 22 samples were collected from the Hetang Formation in southern Anhui province in the Lower Yangtze area, 53 samples from the Hetang Formation in western Zhejiang province, 20 samples from the Mufushan Formation in northern Jiangsu province, and 9 samples from the Wangyinpu Formation in northwest Jiangxi province. Previous well data (well locations are shown in Figure 1) were also collected to investigate the factors that control the enrichment and accumulation of lower Cambrian shale gas in the Middle and Lower Yangtze River regions.

3.2. Methods

For each sample, about 100 g of fresh rock was carefully crushed into gravel-sized particles using a sturdy steel jaw crusher. The particles were then pulverized to a fine powder with a mesh size finer than 200 in an agate mortar, after which the powdered samples were divided into several fractions for geochemical and mineralogical analyses.

Total organic carbon (TOC) analyses were carried out in the Experimental Research Center (ERC) of Yangtze University. For each experiment, 200 mg of powder was treated with 10% hydrochloric acid (HCl) at a temperature of 60 °C to eliminate carbonates. The sample was then washed with distilled water to ensure the complete removal of any residual HCl. The residue was dried and the TOC was analyzed using a Leco CS-230 carbon and sulfur analyzer with an accuracy of $\pm 0.5\%$. The consistency was confirmed by repeating the experiments in accordance with the Chinese national standard [60]. Vitrinite reflectance (R_o) tests were carried out at the ERC on an MPV-SP microphotometer under oil immersion, with more than ten readings for each sample.

Mineralogical analyses were conducted at the ERC on randomly oriented rock powder samples using a HUBER MC 9300 X-ray diffraction (XRD) instrument. The analysis procedure and data evaluation methodologies followed those of [61].

Stable carbon isotope analyses were conducted using a Finnigan MAT-253 instrument at the ERC of Yangtze University. The stable carbon isotope data were expressed in δ -notation ($\delta^{13}\text{C}$, ‰) and referenced against the V-PDB standard with a precision of $\pm 0.5\%$.

Field-emission scanning electron microscopy (FE-SEM) was carried out at the Experimental Center, iRock Technology Co., Ltd., Beijing, China, using a Thermo Fisher Helios G5CX (FE-SEM) with secondary electron imaging and electron backscatter diffraction. The samples were prepared via argon ion milling prior to the pore structure observation using FE-SEM.

Isothermal adsorption was carried out at the Research Institute of Exploration and Development of the North China Oilfield. An ISO 300 isothermal adsorption instrument was used, with an experimental temperature of 30 °C and a methane gas concentration of 99.999%.

In addition, 192 samples were collected for major element analysis, with the source of silicon being determined by calculating the excess siliceous content (Si_{ex}) (the content of siliceous minerals other than regular terrigenous clastic deposits), which was determined according to the following formula:

$$\text{Si}_{\text{ex}} = \text{Si}_s - (\text{Si}/\text{Al})_{\text{bg}} \times \text{Al}_s \quad (1)$$

where Si_s represents the elemental silicon content in the sample, and Al_s is the elemental aluminum content. The obtained value for $(\text{Si}/\text{Al})_{\text{bg}}$ was 3.11, which is the average content observed in shales [26].

4. Results

4.1. Total Organic Carbon (TOC) and Vitrinite Reflectance (R_o)

The TOC and R_o of fifty samples from the Lower Yangtze region were tested. The TOC of the samples from HTC in the Lower Yangtze region was 0.11–17.72 wt.% (average 7.67 wt.%), with an R_o of 3.84%–5.08% (average 4.62%); the TOC of the samples from LY was 0.16–14.30 wt.% (average 4.01 wt.%), with an R_o of 2.57%–4.41% (average 3.73%); the TOC of the samples from DB was 0.19–15.10 wt.% (average 4.29 wt.%), with an R_o of 2.76%–3.76% (average 3.13%); the TOC of the samples from XY-1 was 3.13–17.18 wt.% (average 11.0 wt.%), with an R_o of 3.20%–4.66% (average 4.19%); the TOC of the samples from JJD was 8.29–25.10 wt. % (average 14.02 wt. %), with an R_o of 3.06%–3.85% (average 3.47%); see Table S1.

The TOC and R_o data for the lower Cambrian marine shale in the Middle and Lower Yangtze regions from previous studies are summarized in Table S1. As shown in Figure 3a, the average TOC values for both regions were greater than 1.5%, but the TOC value in the Lower Yangtze region was significantly higher than that in the Middle Yangtze region (see Figure 3a). The R_o of the lower Cambrian marine shale in both the Middle and Lower Yangtze regions was greater than 2%, indicating that the organic matter entered the overmature stage. However, the degree of thermal evolution in the Lower Yangtze region was significantly greater than in the Middle Yangtze region (see Figure 3b).

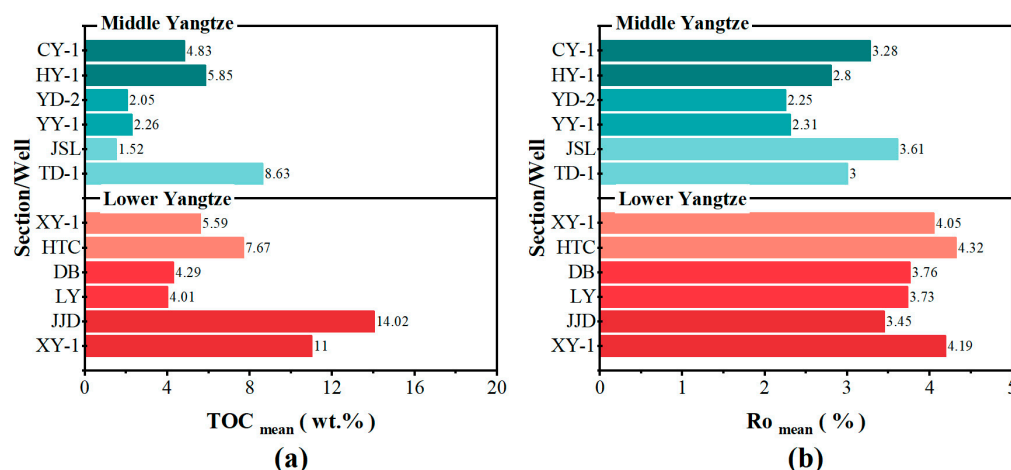


Figure 3. Comparison of the organic geochemical characteristics of the lower Cambrian marine shale in the Middle and Lower Yangtze areas. (a) TOC; (b) R_o . The average values of TOC and R_o in the organic-rich shale of the lower Cambrian in the Lower Yangtze area were higher than those in the Middle Yangtze area. The data for wells CY-1, HY-1, YD-2, YY-1, TD-1, XY, and the JSL section were taken from references [46,58,59,62–65], respectively.

4.2. Carbon Isotope and Organic Matter Types

The $\delta^{13}C$ values for six shale samples from the lower Cambrian Shuijingtuo Formation in the Central Yangtze region ranged from -32.71‰ to -29.23‰ , confirming that they belonged to type I and type III1 kerogens. The $\delta^{13}C$ values for nine shale samples from the lower Cambrian Hetang Formation in the Lower Yangtze region ranged from -36.72‰ to -30.72‰ , which all belonged to type I kerogens (Table S1).

4.3. Mineralogy

In the Lower Yangtze region, the HTC and TLL samples from the Hetang Formation shale showed high clay mineral contents, ranging from 35.0 to 41.0% (average 38.4%) and 41.0 to 51.0% (average 44.8%), respectively. The quartz contents of these samples were comparatively low, ranging from 31.0 to 48.0% (average 39.4%) and 31.0 to 37.0% (average 34.8%), respectively. However, the Hetang Formation shale in DT and LY had higher quartz contents—ranging from 71.7 to 85.9% (average 75.8%) and 53.6 to 86.3% (average 76.1%),

respectively—but lower clay mineral contents, ranging from 7.4 to 13.5% (average 11.2%) and 6.4 to 20.5% (average 11.7%), respectively. The carbonate contents of all these samples were low. Previous research data on the mineral composition of the lower Cambrian marine shales are summarized in Table S2, with the data indicating that the lower Cambrian marine shales in the Middle Yangtze region had high calcium and low silicon contents, while the shales in the Lower Yangtze region had high silicon and low calcium contents (Figure 4).

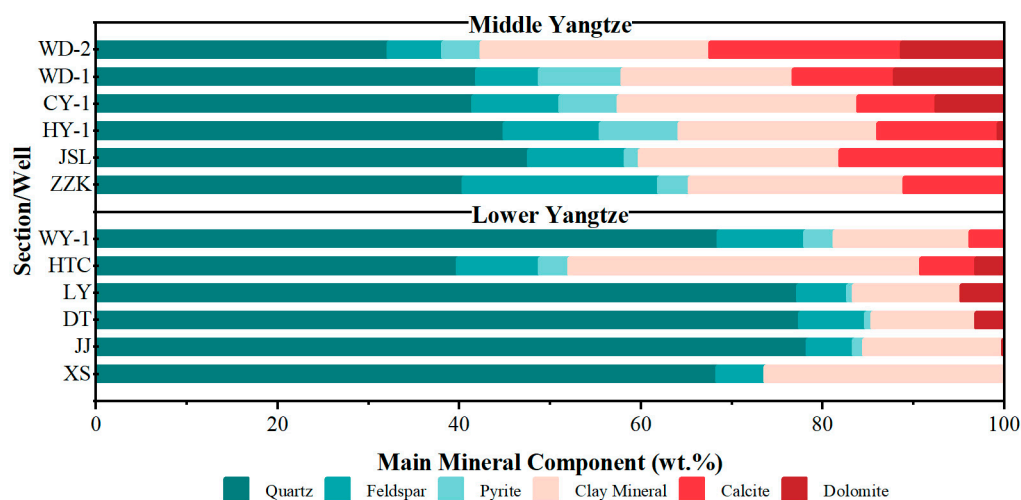


Figure 4. Comparison of the bulk rock mineral compositions of the lower Cambrian marine shales in the Middle and Lower Yangtze areas. The carbonate content in the lower Cambrian shale in the Middle Yangtze region was higher than that in the Lower Yangtze region, whereas the quartz content was significantly lower. The data for wells CY-1 and HY-1 were from reference [58], the data for wells WD-1 and WD-2 were from reference [43], the data for the JSL and ZZK sections were from reference [66], the data for well WY-1 were from reference [46], the data for the JJ section were from reference [67], and the data for the XS section were from reference [68].

4.4. Isothermal Adsorption

4.4.1. Nitrogen Isothermal Adsorption

The nitrogen adsorption hysteresis regression curves of the samples from the lower Cambrian Hetang Formation in the Lower Yangtze region were all H₃-type hysteresis loops according to the IUPAC classification, corresponding to parallel plate-like pores [69,70]. The shale samples from the Hetang Formation showed small adsorption amounts in the low-pressure region, indicating a small number of micropores. The absence of a saturation trend in P/P₀ suggests the presence of large pores that had not been filled [69]. The BJH total pore volumes of the mud shale samples from well XY-1, DT, LY, and FC sections were 0.012~0.015 cm³·g⁻¹ (average 0.013 cm³·g⁻¹), 0.011~0.014 cm³·g⁻¹ (average 0.013 cm³·g⁻¹), 0.012~0.015 cm³·g⁻¹ (average 0.014 cm³·g⁻¹), and 0.014 cm³·g⁻¹, respectively; the BET specific surface areas were 3.62~4.69 m²·g⁻¹ (average 4.16 m²·g⁻¹), 2.67~3.98 m²·g⁻¹ (average 3.33 m²·g⁻¹), 3.62~5.95 m²·g⁻¹ (average 4.79 m²·g⁻¹), and 4.66 m²·g⁻¹, respectively; and the BJH average pore sizes were 13.07~13.78 nm (average 13.43 nm), 14.68~20.28 nm (average 17.48 nm), 9.01~13.07 nm (average 11.04 nm), and 10.98 nm, respectively. The results of previous studies of the mineral composition of lower Cambrian marine shale in the middle and lower Yangtze regions are summarized in Table 1.

The principal differences in the pore traits of the lower Cambrian marine shale across the Middle and Lower Yangtze regions lay in the pore size, volume, and specific surface area. A comparison with data from previous studies indicates that the lower Cambrian marine shale in the Middle Yangtze region had a greater total BJH pore volume and BET-specific surface area, while the average BJH pore size was smaller than that in the Lower Yangtze region (Table 1).

Table 1. Comparison of the reservoir physical properties (including BJH total pore volume ($\text{cm}^3 \cdot \text{g}^{-1}$), BET specific surface area ($\text{m}^2 \cdot \text{g}^{-1}$), and BJH average pore diameter (nm)) of the lower Cambrian marine shale in the Middle and Lower Yangtze regions.

Region	Section	Formation	Physical Characteristics of Shale Reservoirs			Data Sources
			BJH Total Pore Volume/ $(\text{cm}^3 \cdot \text{g}^{-1})$	BET Specific Surface Area/ $(\text{m}^2 \cdot \text{g}^{-1})$	BJH Average Pore Diameter/(nm)	
Middle Yangtze	WD-1	Shuijingtuo	0.007~0.044/0.017 *	5.94~25.72/11.08	5.42~7.86/6.85	[43]
	WD-2	Shuijingtuo	0.011~0.039/0.021	10.67~19.8/14.75	6.14~7.71/7.07	[43]
	HY-1	Suijingtuo	0.001~0.020/0.008	0.80~27.54/8.11	3.84~8.80/5.32	[71]
Lower Yangtze	XC	Hetang	0.006~0.010/0.008	2.15~8.89/5.65	4.21~14.3/7.63	[39]
	XY-1	Hetang	0.006~0.012	4.30~7.50	No data	[46]
	DT	Hetang	0.012~0.015/0.013	3.62~4.69/4.16	13.07~13.78/13.43	This study
	LY	Hetang	0.011~0.014/0.013	2.67~3.98/3.33	14.68~20.28/17.48	This study
	FC	Hetang	0.012~0.015/0.014	3.62~5.95/4.79	9.01~13.07/11.04	This study
	XY-1 RDZ01	Wangyinpu Wangyinpu	0.014 0.005~0.018/0.008	4.66 1.84~9.19/5.23	10.98 4.76~21.21/9.63	This study [72]

Note: * number 1~number 2/number 3 represent min~max/mean, respectively.

4.4.2. Methane Isothermal Adsorption

Linear regression was applied to compare the adsorption capacities of the lower Cambrian marine shales in the middle and lower Yangtze regions [73]. Their Langmuir volumes (V_L) were calculated based on the isothermal adsorption curve of methane (see Table 2). The range of V_L for the samples from the middle Yangtze region was 1.16~8.19 m^3/t (average 2.73 m^3/t); the range of V_L for the samples in the lower Yangtze region was 0.50~16.87 m^3/t (average 5.42 m^3/t).

Table 2. The adsorption capacity (V_L (m^3/t)) of lower Cambrian marine shale in the Middle and Lower Yangtze regions.

Region	Sample	TOC (%)	V_L (m^3/t)	Region	Sample	TOC (%)	V_L (m^3/t)
Middle Yangtze	ZZK-1	0.58	1.16	Lower Yangtze	LWD-1	2.49	2.86
	ZZK-2	1.73	1.84		AR-1	1.19	1.22
	MR-1	0.81	2.77		YZJ-1	3.98	4.47
	MR-2	1.49	1.72		YZJ-2	5.37	5.69
	XLC-1	0.88	1.74		FC-1	0.09	0.62
	XLC-2	1.02	2.00		FC-2	7.35	8.6
	XLC-3	1.65	1.89		DT-1	0.24	0.5
	MXK-1	0.97	2.03		DT-2	0.09	0.92
	MXK-2	13.13	8.19		DT-3	3.03	4.06
	JSL-1	1.36	1.72		DT-4	2.01	2.03
	JSL-2	2.36	2.47		LY-1	14.3	15.95
	JSL-3	1.54	2.46		LY-2	5.26	6.65
	WJP-1	1.45	2.01		LY-3	8.94	16.87
	WJP-2	2.99	2.90				
	SFJ-1	10.96	6.09				

4.5. Pore Types Identified by FE-SEM

Shale pores can be divided into intergranular pores, intragranular pores, organic matter pores, and microfractures [74], with the organic components of micropores being the main controlling factors for gas adsorption [75]. Figure 5 shows the pore characteristics of the marine shale of the Shuijingtuo Formation in the Luojiacun (LJC) section, Zigui County, in the Yichang area of the Middle Yangtze area, under a field emission scanning electron microscope (FE-SEM). Both the organic and inorganic pores were generally well developed, with the inorganic pores being predominantly dissolution pores in carbonate minerals. Spongy micropores had developed in the organic matter, and microfractures

occurred in the interiors and at the edges of the organic matter. Figure 6 shows the FE-SEM pore characteristics of marine shale in the Hetang Formation in the Hongtaocun (HTC) Section in Shitai County, southern Anhui Province. Under the microscope, large amounts of interstitial and bulk organic matter could be observed, but organic and inorganic pores were less developed. A small number of isolated organic pores occurred sporadically in organic matter, mostly flat and irregular in shape, with obviously high long-axis/short-axis ratios and collapsed edges. Inorganic pores occurred as clay mineral intercrystalline pores, potash feldspar intragranular solution pores, and other types. Organic pores and intragranular carbonate solution pores were well developed in the Middle Yangtze area, while inorganic pores were the main pore types in the Lower Yangtze area, where organic pores were comparatively underdeveloped.

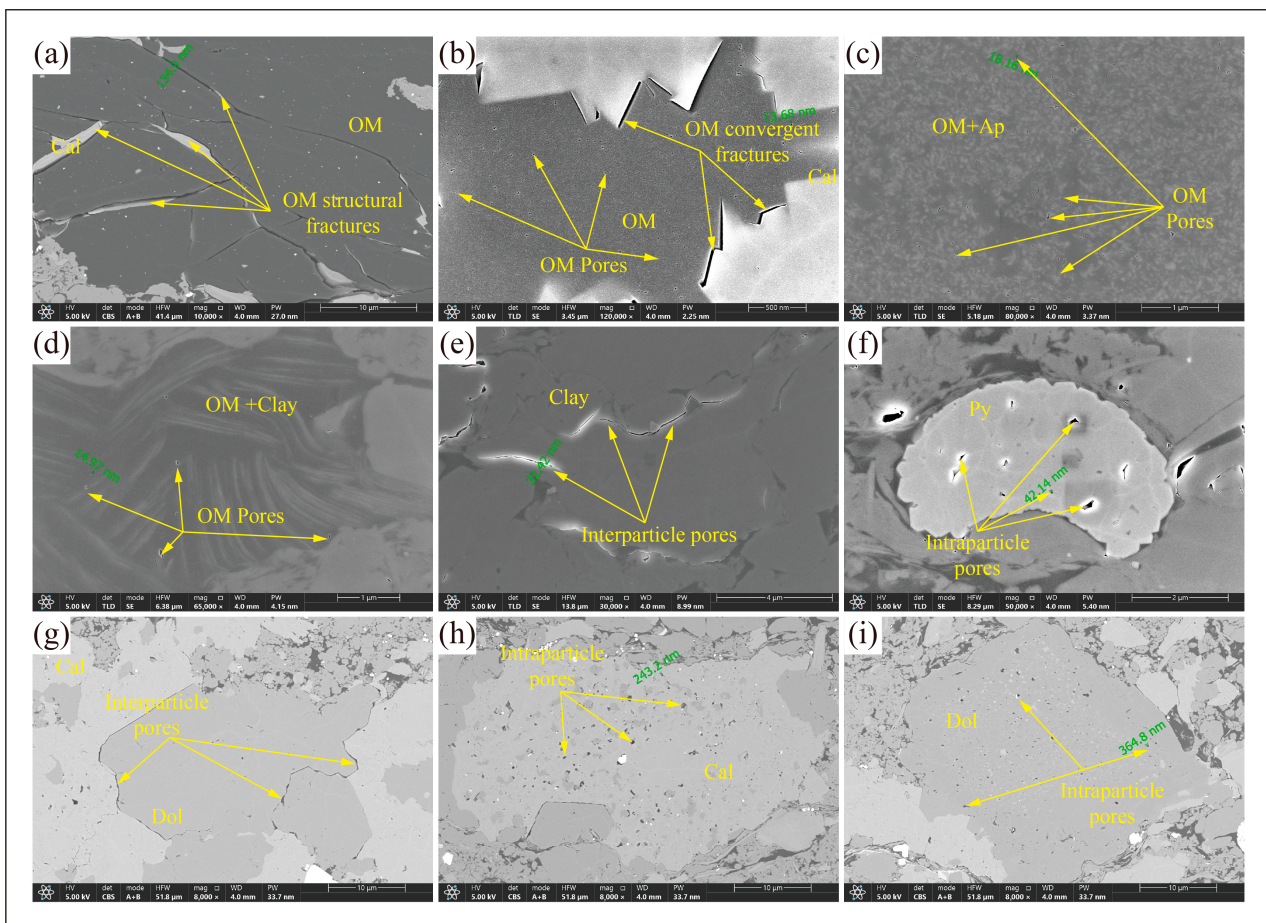


Figure 5. Pore characteristics of marine shale in the lower Cambrian Shuijingtuo Formation in the Luojiacun section (LJC), Zigui County, Yichang City, Middle Yangtze. The lithology of the test sample was black shale, TOC was 4.07 wt. % and R_o was 3.16%, with observation using FE-SEM. (a) The block-like organic matter shows visible shrinkage fissures, which were filled with calcite. (b) The block-like organic matter contains many sponge-like organic micropores internally, with the edges showing shrinkage fissures. (c) The organic matter was mixed with phosphorite, and many sponge-like organic micropores were developed. (d) The organic matter was mixed with clay minerals, with a small number of isolated organic micropores having developed. (e) Interlayer pores of clay minerals. (f) Pores between strawberry-like goethite grains. (g) Pores between mineral grains. (h) Calcite grains show a large number of dissolution pores internally. (i) Dolomite grains show a large number of dissolution pores internally. OM—organic matter, Qtz—quartz, Cal—calcite, Dol—dolomite, Py—pyrite, Ap—apatite, Kfs—K-feldspar.

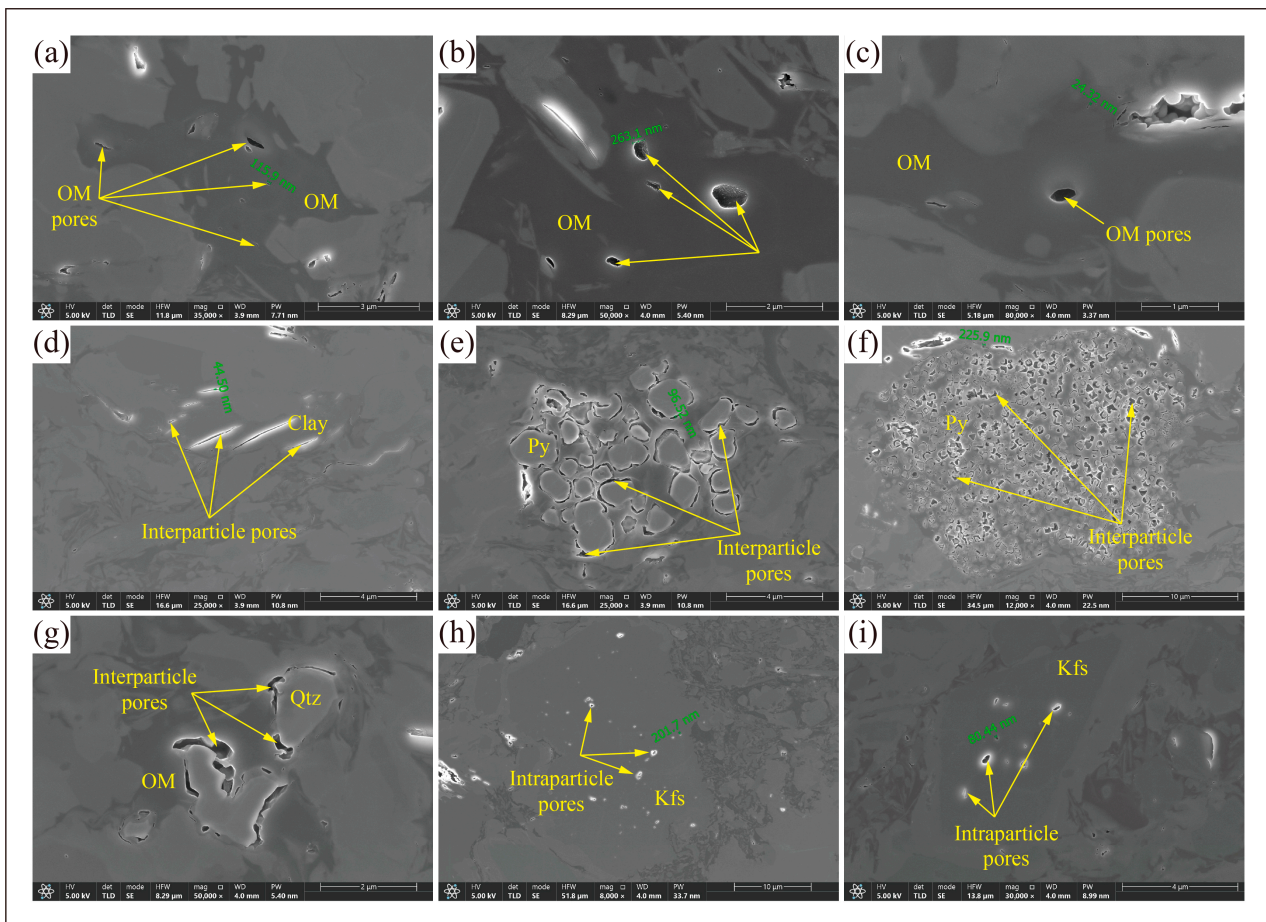


Figure 6. Pore characteristics of lower Cambrian Hetang Formation Marine Shale in the Hongtaocun Section (HTC), Shitai County, Southern Anhui Province, Lower Yangtze Region. The lithology of the test sample was carbonaceous shale, TOC was 7.59 wt. % and R_o was 3.86%, with observation using FE-SEM. (a–c) Dispersed blocky organic matter and infilled organic matter developed sporadic pores, which were relatively large. The developed organic matter pores mostly exhibited a flattened irregular shape, with a significantly higher long-axis/short-axis ratio and collapsed edges. (d) Interlayer pores of clay minerals. (e,f) Intergranular pores between straw-like goethite particles. (g) Intergranular pores between mineral grains. (h,i) Alteration of potassium feldspar along the edges, with the development of intragranular dissolution pores. OM—organic matter, Qtz—quartz, Cal—calcite, Dol—dolomite, Py—pyrite, Ap—apatite, Kfs—K-feldspar.

5. Discussion

5.1. The Source of Silicon and Its Controlling Effect on the Quality of Early Cambrian Marine Shale

The hydrocarbon-generating capacities of different types of organic matter vary. Type I kerogens have greater hydrocarbon-generation potentials [76,77]. The kerogen type of the Lower Yangtze shale is type I, and thus, the hydrocarbon generation potential of the lower Cambrian marine shale in that area is generally high. In addition, the abundance of organic matter is the material basis for the accumulation of shale gas [55,56]. Both areas had relatively high TOC contents, with average values exceeding 1.50 wt. % (see Figure 3a), providing the material basis for shale gas generation. TOC contents in the Lower Yangtze area were significantly higher than in the Middle Yangtze area (see Figure 3a), indicating that the Lower Yangtze area had a better material basis for hydrocarbon generation. Greater organic richness facilitates the generation of more shale gas and is also more effective in generating porosity during the cracking process [77].

Analysis of mineral composition is an indispensable element in shale reservoir research and an important basis for the study of shale gas adsorption and storage, fracture evaluation, percolation and migration, fracturing, and technological properties [34,35,78,79]. Contents of brittle minerals (such as quartz, feldspar, and calcite) are important factors in controlling the degree of fracture development, which directly affects the reservoir space and percolation channels [80]. It also forms a rigid supporting framework, which is beneficial for the preservation of organic and inter-crystalline pores in clay minerals [43]. In addition, an increase in brittle mineral contents makes it more likely that network cracks will form, which is conducive to fracturing [81].

The brittle mineral contents of the Barnett and Woodford shales, which meet industrial development conditions abroad, are generally more than 40% [82]. The brittle mineral content of the organic-rich marine shale in the early Cambrian in the Middle and Lower Yangtze areas was more than 40%, and the average content was more than 60% (see Figure 4), indicating high brittleness and good fracturability [83,84]. However, there were some differences in the proportions and types of brittle minerals in the early Cambrian shales in different areas. The brittle minerals in the shales in the Middle Yangtze area were higher in calcium and lower in silicon than in the Lower Yangtze area (Figure 4). Across the Middle and Lower Yangtze areas, carbonate minerals generally decreased while siliceous minerals increased (see Figure 7a).

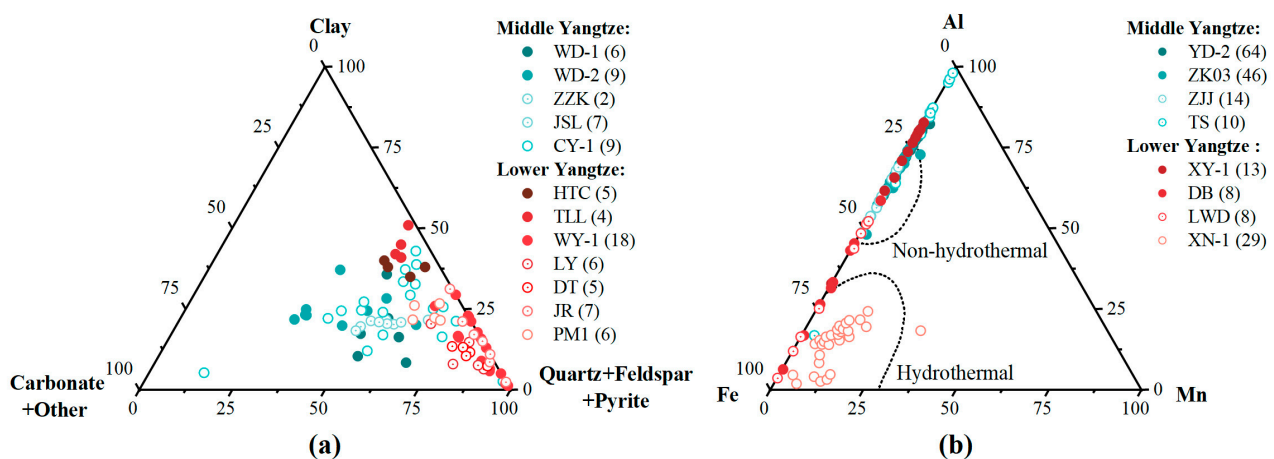


Figure 7. (a) Ternary diagram of the mineral components of the lower Cambrian marine shales in the Middle and Lower Yangtze areas, with the base map drawn from [85]. The data for wells WD-1 and WD-2 were from reference [43], the data for the ZZK and JSL sections were from reference [66], and the data for wells CY-1 and WY-1 were from references [46,58], respectively. The data for the JR and PM1 sections were from references [67,86], respectively. (b) Ternary diagram of Al-Fe-Mn for the lower Cambrian marine shales in the Middle and Lower Yangtze areas reflects the sources of silica. The base map was from reference [16,17]. The data for wells YD-2, ZK03, XY-1, and XN-1 were from references [19,30,44,87], respectively. The data for the ZJJ and TS sections were from references [88,89], respectively.

In the early Cambrian, the water depth of the Yangtze Plate increased from the northwest to the southeast [28,29]. The water body in the Middle Yangtze region was relatively shallow (Figure 1), and thus, there were more calcareous components in the sedimentary rocks. However, the sources of siliceous material in the sediment were mainly terrigenous clastic, hydrothermal fluid, and biogenic [25,90–92]. Excessive silica (SiO_2_{ex}) is often used to characterize the SiO_2 content above that of normal clastic sedimentation [25], which is caused by hydrothermal fluids and biogenesis [93,94].

The Al-Fe-Mn ternary diagram is often used to indicate the origin of additional silicon [17]. Figure 7b shows that the sample points in the Middle Yangtze region almost all fell in areas with non-hydrothermal origins, while the sample points in the Lower Yangtze region mostly fell in areas with hydrothermal origins. This indicates that the Si_{ex} in the

Lower Yangtze region was more significantly affected by hydrothermal fluids, and it also indicates that hydrothermal activity in the Lower Yangtze region was more widespread and frequent than in the Middle Yangtze region during the early Cambrian. Figure 8a shows a good positive correlation between Si_{ex} and TOC in the Middle Yangtze region ($R^2_{YD-2} = 0.53$, $R^2_{ZK03} = 0.61$), reflecting a biogenic origin for Si_{ex} . Figure 8b shows no significant correlation between Si_{ex} and TOC in the Lower Yangtze region, indicating a non-biogenic origin for Si_{ex} , which supports the results shown in the Al-Fe-Mn ternary diagram, which indicate that the Si_{ex} in the Lower Yangtze shale came from hydrothermal fluids.

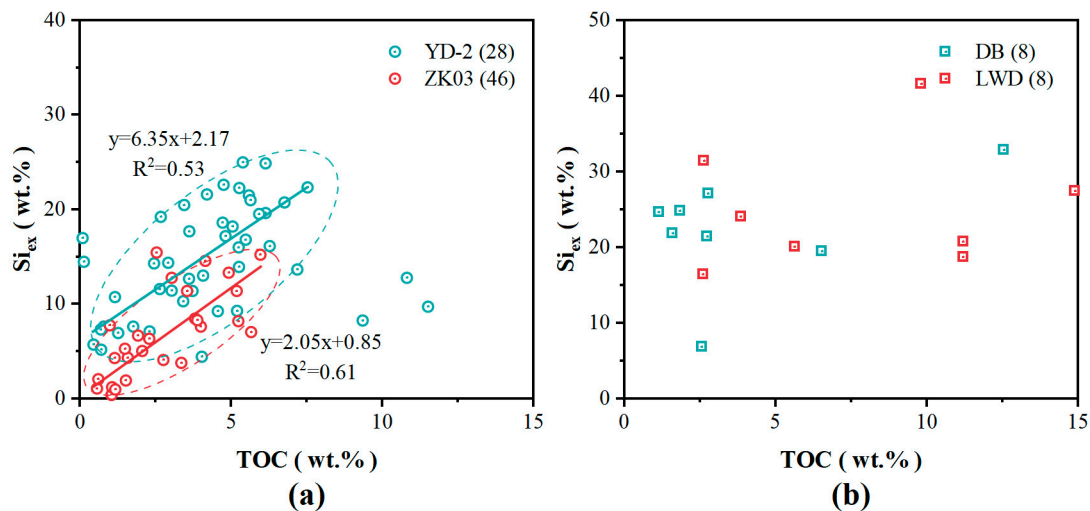


Figure 8. Cross-plot of Si_{ex} and TOC in the lower Cambrian marine shales in the Middle and Lower Yangtze areas, with (a) representing the Middle Yangtze area and (b) representing the Lower Yangtze area. The data for wells YD-2 and ZK03 were from references [19,44], respectively, while the data for the DB and LWD sections were from reference [28]. In the Middle Yangtze area, there was a strong positive correlation between Si_{ex} and TOC, indicating that the silica was primarily of biogenic origin. However, in the Lower Yangtze area, there was no significant linear correlation between Si_{ex} and TOC, suggesting that the silica was primarily derived from hydrothermal fluids.

Hydrothermal fluid activity was, therefore, the main factor that caused the higher silica content in the shale of the Lower Yangtze region. The large amounts of nutrients carried by hydrothermal fluids lead to increased marine productivity [79,80] and increased organic carbon deposition flux, which is more favorable for organic matter enrichment [95]. This explains the higher TOC content in the shale in the Lower Yangtze region, where hydrothermal activity during deposition was the main factor in causing greater enrichment of the organic matter, as well as a higher brittle mineral quartz content.

5.2. Reservoir Physical Property Differences and Its Control Factors

The total pore volume and BET specific surface area of the lower Cambrian marine shale in the Middle Yangtze region were comparatively large (Figure 1), which theoretically provided more adsorption sites for the shale. However, comparing the TOC and the BET specific surface areas and total pore volumes in the Middle and Lower Yangtze regions (Figure 9), it was found that there was no significant linear relationship between the TOC content and the specific surface area and total pore volume in the shale of the Middle Yangtze region (Figure 9a,b), indicating that organic matter pores were not the main contributor to the micropore volume and specific surface area. However, the TOC content of the shale in the Lower Yangtze region did show a significant positive correlation with the specific surface area and total pore volume, indicating that the micropore volume and specific surface area were mainly provided by organic matter pores (Figure 9c,d). As shown in Figure 5, a large number of carbonate intragranular dissolution pores developed

in the shale of the Middle Yangtze region, and thus, the micropore volume and specific surface area in that region were mainly provided by organic matter pores and carbonate intragranular dissolution pores. However, shale gas is generally adsorbed in organic matter pores [1]. The pores of the lower Cambrian marine shale in the Middle Yangtze region were more developed and possessed substantially larger specific surface areas, which suggests that the “effective” specific surface area of pores—the area with the ability to adsorb shale gas—was smaller in the Middle Yangtze region than in the Lower Yangtze region.

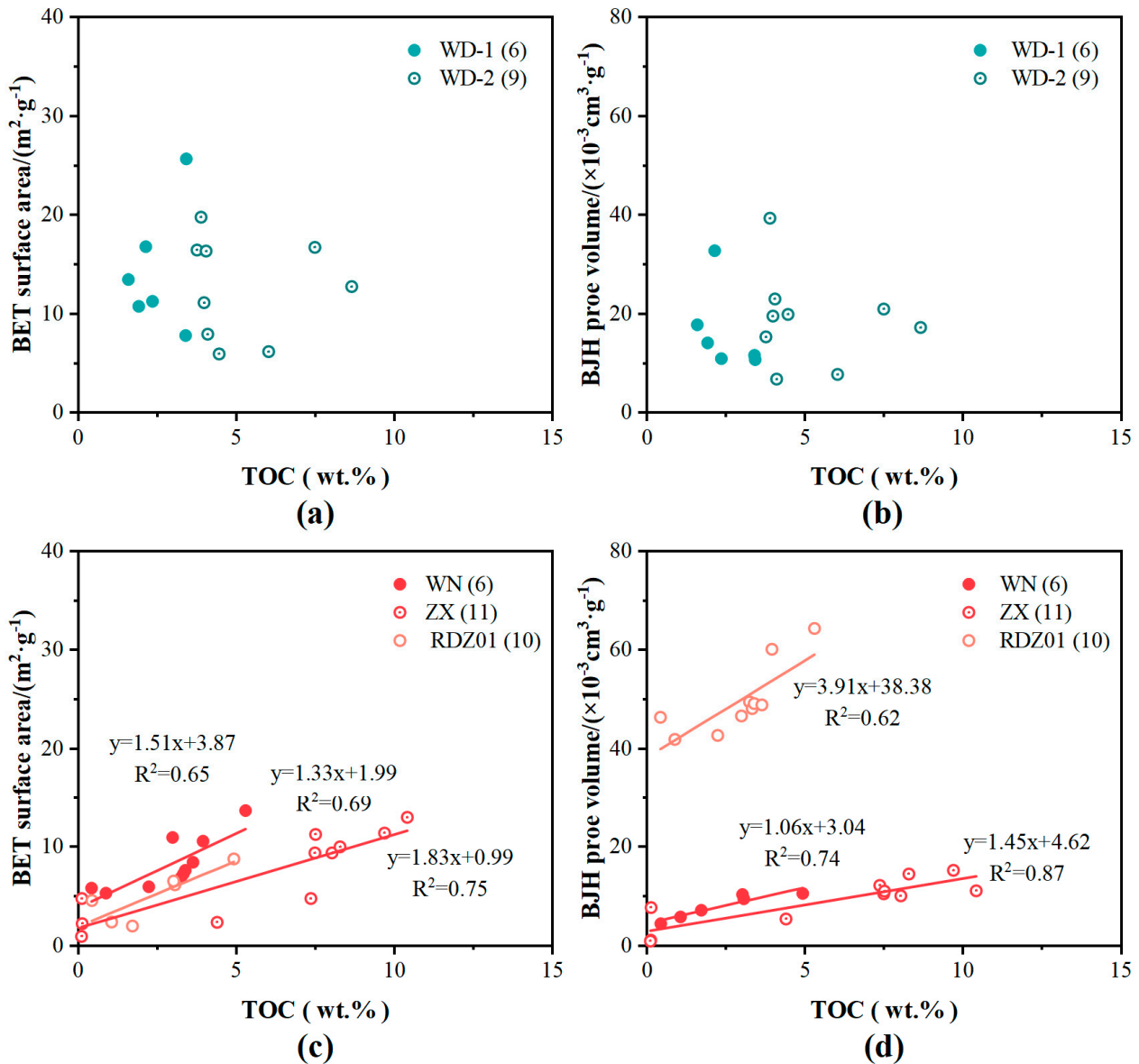


Figure 9. Cross-plot of TOC, BET specific surface area, and BJH pore volume for the lower Cambrian marine shales in the Middle and Lower Yangtze areas. There was no significant correlation between TOC and BET specific surface area (a) or between TOC and BJH pore volume (b) in the Middle Yangtze area. However, a significant positive correlation was observed between TOC and BET specific surface area (c) and between TOC and BJH pore volume (d) in the shales of the Lower Yangtze area. The data for wells WD-1 and WD-2 were from reference [43], the data for the WN section were from reference [39], and the data for well RDZ01 were from reference [72].

From the perspective of sedimentary–tectonic evolution, the Middle and Lower Yangtze regions experienced strong tectonic deformation from the end of the Paleozoic to the Mesozoic [96]. However, the tectonic activity and magma intrusion in the Lower

Yangtze region were more intense than in the Middle Yangtze region [84,85], and the thickness of the Mesozoic strata in the Lower Yangtze region is greater than in the Middle Yangtze region, especially in the southern Anhui region, where it can reach 20,090 m [96]. Strong tectonic deformation and deep burial depths significantly affect the development and preservation of shale pores [97,98].

Strong tectonic and magmatic activity generates large numbers of fractures in shale, which leads to a deterioration in the sealing ability of the hydrocarbon generation system and strengthening of the organic matter condensation reactions, resulting in dense shale with reduced porosity. At the same time, the fluid that originally filled the pores will escape and dissipate in large quantities due to fractures and magmatic channels [98]. However, the formation pressure generated by the thick upper overburden layer will compress or collapse organic pores without fluid filling and compress or compact the interlayer pores of clay minerals [98]. In addition, it was found in exploration practice that under deep, high-temperature, and high-pressure conditions, the brittle–ductile transition zone of shale gradually merges into the ductile zone, and the plasticity of the shale increases while its compressive strength decreases, which is extremely detrimental to the development and preservation of pores [99–101]. These factors have resulted in reduced pore development in the lower Cambrian marine shale in the Lower Yangtze region compared with the Middle Yangtze region.

5.3. Differences in Shale Gas-Bearing Properties and Controlling Factors

The cross-plot of V_L and TOC of the lower Cambrian marine shale in the Middle and Lower Yangtze regions (Figure 10) shows that both TOC and V_L show good positive correlations in the Middle and Lower Yangtze regions, indicating that TOC was an important factor in controlling the adsorption capacity of shale. In addition, when the TOC values are similar, the V_L of the lower Cambrian marine shale in the Lower Yangtze region was larger than that of the Middle Cambrian marine shale in the Middle Yangtze region (in Figure 10, the slope of the fitting curve for the Lower Yangtze samples was significantly greater than that of the Middle Yangtze samples), indicating that the adsorption capacity of the lower Cambrian marine shale in the Lower Yangtze region was greater.

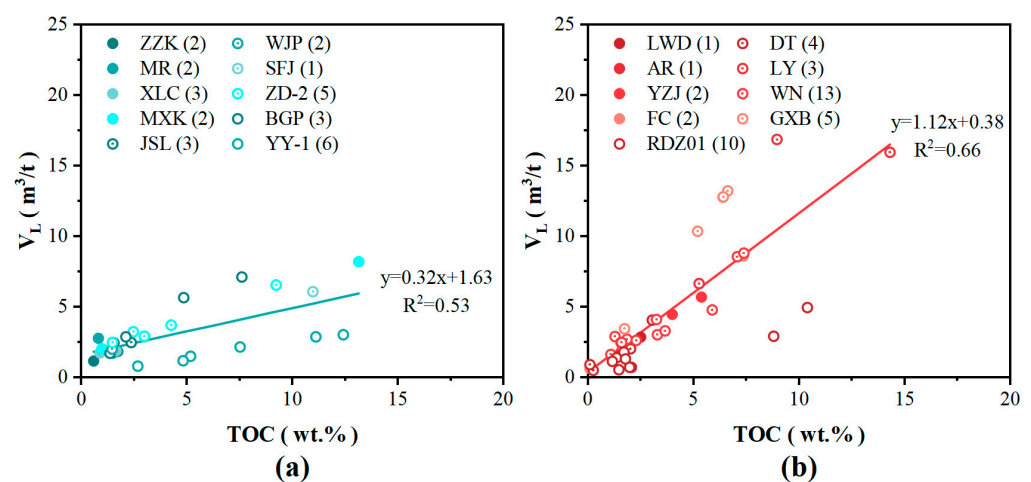


Figure 10. Cross-plot of V_L versus TOC data for the lower Cambrian marine shale in the Middle and Lower Yangtze areas. (a) represents the Middle Yangtze area and (b) represents the Lower Yangtze area. The TOC and V_L in both regions showed good positive correlations, but there were still differences between them. The variation in V_L with TOC in the Lower Yangtze area was more significant than in the Middle Yangtze area, indicating that the content of TOC exerted stronger control over V_L (adsorption capacity). Specifically, the data for ZD-2, BGP, YY-1, WN, GXB, and RDZ01 were from references [36–41], respectively. The other data were from this study.

The pores of the lower Cambrian marine shale in the Middle Yangtze area were more developed (see Figures 5 and 6), and their specific surface areas were significantly larger than those in the Lower Yangtze area (see Table 1). However, the adsorption capacity (V_L) of mud shale was significantly inferior to that of the Lower Yangtze region. This indicates that the “effective” specific surface area of the pores capable of adsorbing shale gas was smaller in the Middle Yangtze area than in the Lower Yangtze area. The thermal evolution degree of the organic matter in the shale in the Lower Yangtze area was higher than that in the Middle Yangtze area (see Table S1 and Figure 3b). As the degree of thermal evolution increases, the lipid structure decreases and the aromatic structure increases due to the aromatization of kerogen [98]. However, the aromatic kerogen has a stronger affinity for methane [98], which increases the “effective” specific surface area for methane adsorption, resulting in increased methane adsorption. Changes in the chemical structure of kerogen at high degrees of thermal evolution were therefore among the main factors that controlled the methane adsorption intensity in the lower Cambrian marine shale in the Middle and Lower Yangtze areas.

An increase in carbonate content will also lead to more complex pore structures [43]. The lower Cambrian marine shale in the Middle Yangtze area had a higher carbonate content (see Table S2, Figures 4 and 7a), and thus, it had a more complex pore structure. Previous nitrogen isothermal adsorption experiments on the lower Cambrian marine shale in the Middle and Lower Yangtze areas showed that the nitrogen isothermal adsorption hysteresis loop of the Lower Yangtze area was mostly the H_3 type, while that of the Middle Yangtze area was mostly a combination of the H_2 and H_3 types [36,41,43,72,75,86,102,103]. The shale in the Middle Yangtze area, therefore, had more fine-neck and ink-bottle-like pores, corresponding to organic and dissolution pores [104] and showing poor pore connectivity. Shale with complex pore structures and poor connectivity also has poor methane adsorption performance [105], and thus, the complexity and connectivity of pores were clearly other important factors that controlled the adsorption performance of the lower Cambrian marine shale in the Middle and Lower Yangtze areas.

Although the shale in the Lower Yangtze area has better hydrocarbon generation and reservoir qualities, exploration for shale gas in the area has not made great progress, with exploration and investigation wells typically showing low gas content, low methane content, or no gas content at all [14,43,45,46,106]. In comparison, the shale of the lower Cambrian Shuijingtuo Formation in the Yichang area of the Middle Yangtze area has produced industrial gas flow [14]. Given that the accumulation of shale gas is controlled by both the material nature of the shale and the preservation conditions for shale gas [107], poor preservation conditions are likely to be an important factor that restricted the accumulation of shale gas in the lower Cambrian in the Lower Yangtze area.

5.4. The Influence of Tectonics and Magmatic Activity on the Preservation of Shale Gas

Shale gas reservoirs are generally capable of self-generation and self-storage, and shales that generate shale gas are also reservoirs [35]. Consequently, the sealing ability of the later hydrocarbon generation system will directly affect whether shale gas can be enriched and preserved [35]. The Middle and Lower Yangtze areas are situated within a larger area of strong tectonic deformation [96] (see Figure 11). The stages of tectonic evolution can be divided into a steady subsidence stage before the Indosinian movement, a compressional nappe stage from the Indosinian to the Middle Yanshanian, and an extensional rift stage from the late Yanshanian to the Himalayan.

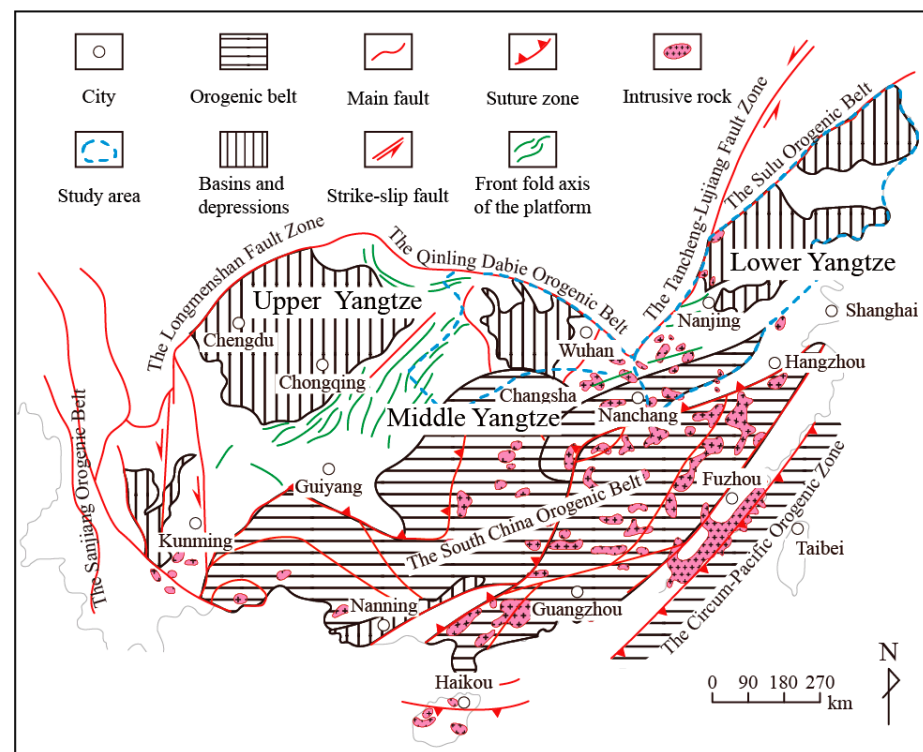


Figure 11. Tectonic division and distribution of intrusive rocks in the Middle and Lower Yangtze areas, modified from references [96,108]. The distribution of intrusive rocks in the Lower Yangtze region is more extensive than in the Middle Yangtze region, where intrusive rocks are mainly confined to the eastern margin close to the Lower Yangtze region.

During the compression and thrusting stage of the Indosinian–Yanshanian period, strong uplift and thrusting caused faulting, strike-slip, folding, and erosion in the Paleozoic strata in the Middle and Lower Yangtze areas. In most areas, the Paleozoic strata were eroded almost completely, with large expanses of Silurian strata exposed. The integrity of the regional cover layers was disrupted, the continuity of the strata was broken, and the development of structural fractures led to the deterioration of reservoir sealing, resulting in the significant loss of shale gas. However, the shielding effect of the Huangling uplift and the ancient basement of Shennongjia meant that there was less structural deformation of the lower Cambrian strata in the Middle Yangtze area than in the Lower Yangtze area [109,110], and therefore, comparatively little destruction of shale gas reservoir traps. Tectonic inversion occurred in the Middle and Lower Yangtze areas during the extensional rift stage from the late Yanshanian to the Himalayan, with the whole area experiencing considerable extension. Most of the reverse faults were reversed into normal faults, and many new normal faults formed. The sealing ability of normal faults is poor [111], and thus, they are not conducive to the preservation of shale gas. However, due to obstruction by the Huangling paleo-uplift, the extension from east to west in the Middle Yangtze area gradually weakened and finally disappeared. In this area, reverse faults turned into normal faults, but new normal faults were relatively few, and shale gas preservation conditions were, therefore, relatively good.

Magmatic activity in the Middle and Lower Yangtze areas primarily occurred during the Yanshan and Himalayan periods and was concentrated in the Lower Yangtze area, particularly in southern Anhui (see Figure 11). Magmatic activity can enhance the permeability of shale to some extent, and, due to the formation of special high-pressure strata, it can enhance its adsorption capacity for shale gas [77,112]. However, in the later stage of reservoir formation, magmatic activity can significantly inhibit the accumulation of shale gas. It can destroy the cap rock, allowing for the intrusive rock pipeline to become a path for shale gas to escape [113]. The intruding high-temperature magma will also bake the surrounding

organic matter, resulting in carbonization or alteration of the mineral composition of the shale, reducing its adsorption capacity for gas [33,114–116]. Due to the particularly intense magmatic activity in the Lower Yangtze region in the later stage of reservoir formation, the damage to the shale gas reservoir and its cap rock was more significant, which is the main reason why exploration for shale gas in this region is particularly challenging.

Generally, strong tectonic deformation and volcanic activity play important roles in the formation and accumulation of shale gas [117]. The development of structural fractures is conducive to shale gas migration, providing more pore space for shale gas attachment, and later, fracturing [107]. However, the destruction of caprock integrity, stratigraphic continuity, and hydrocarbon generation system sealing led to shale gas loss and the excessive thermal evolution of organic matter. Compared with the Middle Yangtze area, stronger tectonic deformation and magmatic activity in the Lower Yangtze area mean that the preservation conditions for shale gas are worse than in the Middle Yangtze area. This is the fundamental reason why shale gas has generally not been preserved in the lower Cambrian strata in the Lower Yangtze area. Finding small-scale, structurally stable areas in the fragmented environment of the Lower Yangtze area is, therefore, the priority for lower Cambrian shale gas exploration in the area.

6. Conclusions

The findings were as follows:

- (1) The organic carbon content of lower Cambrian marine shale in the Lower Yangtze area was markedly higher than that of the Middle Yangtze area, and the thermal evolution degree of organic matter in the Lower Yangtze area was higher than in the Middle Yangtze area.
- (2) The brittle mineral contents of lower Cambrian marine shales in the Middle and Lower Yangtze regions were more than 60%, and they all showed good fracturability. From NW to SE, the types of brittle minerals decreased while siliceous minerals increased. The early Paleozoic marine shale in the Lower Yangtze area had high silicon contents and low calcium contents.
- (3) The adsorption properties of lower Cambrian marine shale in the Lower Yangtze area were better than those in the Middle Yangtze area. However, micropores in the Middle Yangtze shale were more developed than in the Lower Yangtze, indicating that the degree of pore development was not the main factor controlling the adsorption properties of the lower Cambrian marine shale. However, the thermal evolution of organic matter was higher in the Lower Yangtze area, and thus, the proportion of aromatic components in organic matter was higher, and shale gas was therefore more easily absorbed. The particular molecular structure of kerogen caused by high thermal evolution was, therefore, an important factor that controlled the adsorption properties of lower Cambrian marine shale in the Middle and Lower Yangtze regions.
- (4) Strong tectonic deformation and frequent magmatic activity caused the integrity of the regional caprock and the sealing of the hydrocarbon generation system in the Lower Yangtze area to be much poorer than those in the Middle Yangtze area, and thus, the preservation conditions for shale gas were relatively poor. This was the main factor that restricted the accumulation and preservation of lower Cambrian shale gas in the Lower Yangtze area.

Supplementary Materials: The following supporting information can be downloaded from <https://www.mdpi.com/article/10.3390/min14010031/s1>—Table S1: Organic geochemical parameters of the lower Cambrian marine shale in the middle and lower Yangtze region (including organic matter types, TOC (%), and Ro (%)); Table S2: Main mineral component content (%) of the lower Cambrian marine shale in the middle and lower Yangtze region. Refs. [118–121] are cited in Supplementary Materials.

Author Contributions: Conceptualization, D.Z. and H.D.; methodology, H.D.; validation, D.Z., H.D. and Z.D.; investigation, H.D., X.H. and Z.D.; resources, H.D. and Z.D.; writing—original draft

preparation, H.D.; writing—review and editing, D.Z. and X.H.; supervision, D.Z. and X.H.; project administration, D.Z.; funding acquisition, D.Z. All authors have read and agreed to the published version of the manuscript.

Funding: The authors wish to acknowledge the financial support of the National Natural Science Foundation of China (grant no. 42272359) and the Ministry of Natural Resources, P.R.C. (project: evaluation of shale gas resources and selection of favorable areas in the Middle and Lower Yangtze areas).

Data Availability Statement: The original contributions presented in the study are included in the article/supplementary material; further inquiries can be directed to the corresponding authors.

Acknowledgments: We would like to thank Zhanhong Liu, School of Marine Science, China University of Geosciences (Wuhan), for providing samples from the Middle Yangtze area. The authors are grateful for constructive comments by two anonymous reviewers on an earlier draft of this manuscript. We also want to express our gratitude to Shiping Wei from the School of Ocean Sciences of China University of Geosciences (Beijing) for his invaluable support and assistance throughout our research and manuscript revision process. We sincerely appreciate all anonymous reviewers and the handling editor for their critical comments and constructive suggestions.

Conflicts of Interest: The authors declare that the research was conducted in the absence of any commercial or financial relationships that could be construed as potential conflicts of interest.

References

1. Jarvie, D.M.; Hill, R.J.; Ruble, T.E.; Pollastro, R.M. Unconventional Shale-Gas Systems: The Mississippian Barnett Shale of North-Central Texas as One Model for Thermogenic Shale-Gas Assessment. *AAPG Bull.* **2007**, *91*, 475–499. [[CrossRef](#)]
2. John, B. Curtis1 Fractured Shale-Gas Systems. *AAPG Bull.* **2002**, *86*, 1921–1938. [[CrossRef](#)]
3. James, W. Schmoker1 Resource-Assessment Perspectives for Unconventional Gas Systems. *AAPG Bull.* **2002**, *86*, 1993–1999. [[CrossRef](#)]
4. Slatt, R.M.; O'Brien, N.R. Pore Types in the Barnett and Woodford Gas Shales: Contribution to Understanding Gas Storage and Migration Pathways in Fine-Grained Rocks. *AAPG Bull.* **2011**, *95*, 2017–2030. [[CrossRef](#)]
5. Chalmers, G.R.; Bustin, R.M.; Power, I.M. Characterization of Gas Shale Pore Systems by Porosimetry, Pycnometry, Surface Area, and Field Emission Scanning Electron Microscopy/Transmission Electron Microscopy Image Analyses: Examples from the Barnett, Woodford, Haynesville, Marcellus, and Doig Units. *AAPG Bull.* **2012**, *96*, 1099–1119. [[CrossRef](#)]
6. Clarkson, C.R.; Solano, N.; Bustin, R.M.; Bustin, A.M.M.; Chalmers, G.R.L.; He, L.; Melnichenko, Y.B.; Radliński, A.P.; Blach, T.P. Pore Structure Characterization of North American Shale Gas Reservoirs Using USANS/SANS, Gas Adsorption, and Mercury Intrusion. *Fuel* **2013**, *103*, 606–616. [[CrossRef](#)]
7. Wang, X.; Liu, Y.H.; Zhang, M.; Hu, S.Y.; Liu, H.J. Conditions of Formation and Accumulation for Shale Gas. *Nat. Gas Geosci.* **2010**, *21*, 350–356.
8. Zou, C.N.; Dong, D.Z.; Wang, S.J.; Li, J.Z.; Li, X.J.; Wang, Y.M.; Li, D.H.; Cheng, K.M. Geological characteristics, formation mechanism and resource potential of shale gas in China. *Pet. Explor. Dev.* **2010**, *37*, 641–653. [[CrossRef](#)]
9. Zou, C.; Zhai, G.; Zhang, G.; Wang, H.; Zhang, G.; Li, J.; Wang, Z.; Wen, Z.; Ma, F.; Liang, Y.; et al. Formation, Distribution, Potential and Prediction of Global Conventional and Unconventional Hydrocarbon Resources. *Pet. Explor. Dev.* **2015**, *42*, 14–28. [[CrossRef](#)]
10. Cai, X.Y.; Zhou, D.H.; Zhao, P.R.; Zhang, H.; Qian, K.R.; Wang, C.X. Development progress and outlook of deep and normal pressure shale gas of SINOPEC. *Pet. Geol. Exp.* **2023**, *45*, 1039–1049.
11. Zhou, W.; Xu, H.; Yu, Q.; Xie, R.C.; Deng, K. Shale gas-bearing property differences and their genesis between Wufeng-Longmaxi Formation and Qiongzhusi Formation in Sichuan Basin and surrounding areas. *Lithol. Reserv.* **2016**, *28*, 18–25.
12. Dong, D.Z.; Cheng, K.M.; Wang, Y.M.; Li, X.J.; Wang, S.J.; Huang, J.L. Forming conditions and characteristics of shale gas in the Lower Paleozoic of the Upper Yangtze region, China. *Oil Gas Geol.* **2010**, *31*, 288–299+308.
13. Gao, P.; He, Z.; Lash, G.G.; Li, S.; Xiao, X.; Han, Y.; Zhang, R. Mixed Seawater and Hydrothermal Sources of Nodular Chert in Middle Permian Limestone on the Eastern Paleo-Tethys Margin (South China). *Palaeogeogr. Palaeoclimatol. Palaeoecol.* **2020**, *551*, 109740. [[CrossRef](#)]
14. Li, H.; Liu, A.; Luo, S.Y.; Chen, X.H.; Chen, L. Characteristics of the Cambrian Shuijingtuo shale reservoir on Yichang Slope, western Hubei Province: A case study of well EYY 1. *Pet. Geol. Exp.* **2019**, *41*, 76–82. [[CrossRef](#)]
15. Zhao, W.Z.; Jia, A.L.; Wei, Y.S.; Wang, J.L.; Zhu, H.Q. Progress in shale gas exploration in China and prospects for future development. *China Pet. Explor.* **2020**, *25*, 31–44.
16. Wedepohl, K.H. Environmental Influences on the Chemical Composition of Shales and Clays. *Phys. Chem. Earth* **1971**, *8*, 307–333. [[CrossRef](#)]
17. Adachi, M.; Yamamoto, K.; Sugisaki, R. Hydrothermal Chert and Associated Siliceous Rocks from the Northern Pacific Their Geological Significance as Indication of Ocean Ridge Activity. *Sediment. Geol.* **1986**, *47*, 125–148. [[CrossRef](#)]

18. Pan, J.P.; Qiao, D.W.; Li, S.Z.; Zhou, D.S.; Xu, L.F.; Zhang, M.Y.; Song, X.Y. Shale-gas geological conditions and exploration prospect of the Paleozoic marine strata in lower Yangtze area, China. *Geol. Bull. China* **2011**, *30*, 337–343.
19. Zhang, Y.; Huang, D.J.; Zhang, L.L.; Wan, C.H.; Luo, H.; Shao, D.Y.; Meng, K.; Yan, J.P.; Zhang, T.W. Bio gene silica of the lower Cambrian Shui jin gtuao Formation in Yichang, western Hubei Province—Features and influence on shale gas accumulation. *Earth Sci. Front.* **2023**, *30*, 83–100. [[CrossRef](#)]
20. Tréguer, P.; Nelson, D.M.; Van Bennekom, A.J.; DeMaster, D.J.; Leynaert, A.; Quéguiner, B. The Silica Balance in the World Ocean: A Reestimate. *Science* **1995**, *268*, 375–379. [[CrossRef](#)]
21. Siever, R. The Silica Cycle in the Precambrian. *Geochim. Cosmochim. Acta* **1992**, *56*, 3265–3272. [[CrossRef](#)]
22. Steiner, M.; Wallis, E.; Erdtmann, B.-D.; Zhao, Y.; Yang, R. Submarine-Hydrothermal Exhalative Ore Layers in Black Shales from South China and Associated Fossils: Insights into a lower Cambrian Facies and Bio-Evolution. *Palaeogeogr. Palaeoclimatol. Palaeoecol.* **2001**, *169*, 165–191. [[CrossRef](#)]
23. Guo, Q.; Shields, G.A.; Liu, C.; Strauss, H.; Zhu, M.; Pi, D.; Goldberg, T.; Yang, X. Trace Element Chemostratigraphy of Two Ediacaran–Cambrian Successions in South China: Implications for Organosedimentary Metal Enrichment and Silicification in the early Cambrian. *Palaeogeogr. Palaeoclimatol. Palaeoecol.* **2007**, *254*, 194–216. [[CrossRef](#)]
24. Ramseyer, K.; Amthor, J.E.; Matter, A.; Pettke, T.; Wille, M.; Fallick, A.E. Primary Silica Precipitate at the Precambrian/Cambrian Boundary in the South Oman Salt Basin, Sultanate of Oman. *Mar. Pet. Geol.* **2013**, *39*, 187–197. [[CrossRef](#)]
25. Tribouillard, N.; Algeo, T.J.; Lyons, T.; Riboulleau, A. Trace Metals as Paleoredox and Paleoproductivity Proxies: An Update. *Chem. Geol.* **2006**, *232*, 12–32. [[CrossRef](#)]
26. Holdaway, H.K.; Clayton, C.J. Preservation of Shell Microstructure in Silicified Brachiopods from the Upper Cretaceous Wilmington Sands of Devon. *Geol. Mag.* **1982**, *119*, 371–382. [[CrossRef](#)]
27. Yamamoto, K. Geochemical Characteristics and Depositional Environments of Cherts and Associated Rocks in the Franciscan and Shimanto Terranes. *Sediment. Geol.* **1987**, *52*, 65–108. [[CrossRef](#)]
28. Zeng, Z.X. A Study on the Origin and Sedimentary Environment of Siliceous (Shale) Rocks from the Lower Cambrian Hetang Formation in Northwest Zhejiang Province. Master's Thesis, Zhejiang University, Hangzhou, China, 2019.
29. Xu, X.C.; Wang, W.J.; Xiong, Y.P.; Chu, P.L.; Fang, H.B.; Zhao, L.L. REE geochemical characteristics of the lower Cambrian black shale series in Shitai area, Anhui Province, and their geological significance. *Acta Petrol. Mineral.* **2009**, *28*, 118–128.
30. Liu, T.L.; Jiang, Z.X.; Liu, W.W.; Zhang, K.; Xie, X.L.; Yin, L.S.; Huang, Y.Z. Effect of hydrothermal activity on the enrichment of sedimentary organic matter at early Cambrian in the Xiuwu Basin. *Pet. Geol. Recovery Effic.* **2018**, *25*, 68–76. [[CrossRef](#)]
31. Zhu, W.B.; Zhang, X.H.; Qu, Z.D.; Huang, Z.Q.; Wang, X.Q.; Ding, D.L. REE composition and its geological implications of the Hetang Formation mudstones in the East Jiangxi and west Zhejiang, China. *Mar. Geol. Quat. Geol.* **2021**, *41*, 88–99. [[CrossRef](#)]
32. Gao, P.; He, Z.; Lash, G.G.; Zhou, Q.; Xiao, X. Controls on Silica Enrichment of lower Cambrian Organic-Rich Shale Deposits. *Mar. Pet. Geol.* **2021**, *130*, 105126. [[CrossRef](#)]
33. Milliken, K.L.; Esch, W.L.; Reed, R.M.; Zhang, T. Grain Assemblages and Strong Diagenetic Overprinting in Siliceous Mudrocks, Barnett Shale (Mississippian), Fort Worth Basin, Texas. *AAPG Bull.* **2012**, *96*, 1553–1578. [[CrossRef](#)]
34. Pszonka, J.; Schulz, B. SEM Automated Mineralogy applied for the quantification of mineral and textural sorting in submarine sediment gravity flows. *Gospod. Surowcami Miner. Miner. Resour. Manag.* **2022**, *38*, 105–131. [[CrossRef](#)]
35. Zhang, J.C.; Jin, Z.J.; Yuan, M.S. Reservoiring Mechanism of Shale Gas and its distribution. *Nat. Gas Ind.* **2004**, *24*, 15–18+131–132.
36. He, J.; He, S.; Liu, Z.X.; Zhai, G.Y.; Wang, Y.; Han, Y.J.; Wan, K.; We, I.S.L. Pore structure and adsorption capacity of shale in the lower Cambrian Shuijingtuo Formation in the southern flank of Huangling anticline, western Hubei. *Acta Pet. Sin.* **2020**, *41*, 27–42.
37. Zhang, S.Z. Comparison of Geological Conditions of lower Cambrian Shale Gas in the Middle and Lower Yangtze Region. Master's Thesis, China University of Geosciences, Beijing, China, 2018.
38. Long, Y.K. Geological conditions for shale gas accumulation in the Niutitang Formation of the Central Yangtze River region. Jiangnan. *Pet. Sci. Technol.* **2017**, *27*, 7–11.
39. Gao, Y.; Mao, L.; Ma, R. Adsorption characteristics and its controlling factors of organic-rich shales with high thermal maturity. *Sci. Technol. Eng.* **2018**, *18*, 242–248.
40. Wen, M. The Pore Structure Characteristics and Influencing Factors of Lower Paleozoic Marine Shale in the Northwest Jiangxi Region. Master's Thesis, China University of Petroleum, Beijing, China, 2021.
41. Guo, C.L.; Yang, S.; Wang, A.D.; Wang, Y.T.; Zhang, S.L.; Qi, X. Study on the lower Cambrian marine shale reservoir and methane adsorption characteristics in Xiuwu Basin. *Nat. Gas Geosci.* **2021**, *32*, 598–610.
42. Luo, S.Y.; Chen, X.H.; Li, H.; Liu, A.; Wang, C.S. Shale Gas Accumulation Conditions and Target Optimization of lower Cambrian Shuijingtuo Formation in Yichang Area, West Hubei. *Earth Sci.* **2019**, *44*, 3598–3615.
43. Li, H.; Liu, A.; Luo, S.Y.; Chen, X.H.; Chen, L. Pore structure characteristics and development control factors of Cambrian shale in the Yichang area, western Hubei. *Pet. Geol. Recovery Effic.* **2018**, *25*, 16–23. [[CrossRef](#)]
44. Chen, X.H.; Wei, K.; Zhang, B.M.; Li, P.J.; Li, H.; Liu, A.; Luo, S.Y. Main geological factors controlling shale gas reservoir in the Cambrian Shuijingtuo Formation in Yichang of Hubei Province as well as its enrichment patterns. *Geol. China* **2018**, *45*, 207–226.

45. Zhu, W.B.; Zhang, X.H.; Wang, X.Q.; Qu, Z.D.; Huang, Z.Q.; Zhou, D.R. Geological characteristics and shale gas potential of lower Cambrian Hetang Formation in Lower Yangtze region: A case study of Jiangshan—Tonglu area, western Zhejiang province. *Pet. Geol. Exp.* **2020**, *42*, 477–488.
46. Wang, K.M. Geological characteristics and controlling factors of shale gas accumulation of the lower Cambrian in the southern Anhui of Lower Yangtze area. *China Pet. Explor.* **2021**, *26*, 83–99.
47. Shu, L.; Yao, J.; Wang, B.; Faure, M.; Charvet, J.; Chen, Y. Neoproterozoic Plate Tectonic Process and Phanerozoic Geodynamic Evolution of the South China Block. *Earth-Sci. Rev.* **2021**, *216*, 103596. [[CrossRef](#)]
48. Mgimba, M.M.; Jiang, S.; Nyakilla, E.E.; Mwakipunda, G.C. Application of GMDH to Predict Pore Pressure from Well Logs Data: A Case Study from Southeast Sichuan Basin, China. *Nat. Resour. Res.* **2023**, *32*, 1711–1731. [[CrossRef](#)]
49. Shu, L.S. An analysis of principal features of tectonic evolution in South China Block. *Geol. Bull. China* **2012**, *31*, 1035–1053.
50. Veevers, J.J.; Walter, M.R.; Scheibner, E. Neoproterozoic Tectonics of Australia-Antarctica and Laurentia and the 560 Ma Birth of the Pacific Ocean Reflect the 400 M.Y. Pangean Supercycle. *J. Geol.* **1997**, *105*, 225–242. [[CrossRef](#)]
51. Zheng, Y.-F.; Wu, R.-X.; Wu, Y.-B.; Zhang, S.-B.; Yuan, H.; Wu, F.-Y. Rift Melting of Juvenile Arc-Derived Crust: Geochemical Evidence from Neoproterozoic Volcanic and Granitic Rocks in the Jiangnan Orogen, South China. *Precambrian Res.* **2008**, *163*, 351–383. [[CrossRef](#)]
52. Wang, J. History of Neoproterozoic Rift Basins in South China: Implications for Rodinia Break-Up. *Precambrian Res.* **2003**, *122*, 141–158. [[CrossRef](#)]
53. Liu, J.Y.; Zhang, F.Y.; Yin, Y.L. Lithofacies and paleogeographic study on late Cambrian hydrocarbon source rocks in Lower Yangtze Region. *Mar. Geol. Quat. Geol.* **2018**, *38*, 85–95. [[CrossRef](#)]
54. Sahoo, S.K.; Planavsky, N.J.; Kendall, B.; Wang, X.; Shi, X.; Scott, C.; Anbar, A.D.; Lyons, T.W.; Jiang, G. Ocean Oxygenation in the Wake of the Marinoan Glaciation. *Nature* **2012**, *489*, 546–549. [[CrossRef](#)] [[PubMed](#)]
55. Yeasmin, R.; Chen, D.; Fu, Y.; Wang, J.; Guo, Z.; Guo, C. Climatic-Oceanic Forcing on the Organic Accumulation across the Shelf during the early Cambrian (Age 2 through 3) in the Mid-Upper Yangtze Block, NE Guizhou, South China. *J. Asian Earth Sci.* **2017**, *134*, 365–386. [[CrossRef](#)]
56. Wang, H.Z. Early Cambrian Paleogeographic Map of China. In *Atlas of Ancient Chinese Geography*; Beijing Cartography Publishing House: Beijing, China, 1985; pp. 25–26.
57. Feng, Z.S.; Peng, Y.M.; Jin, Z.K.; Jiang, P.L.; Bao, Z.D.; Luo, Z.; Ju, T.Y.; Tian, H.Q.; Wang, H. Cambrian lithofacies and paleogeography in southern China. *J. Palaeogeogr.* **2001**, *3*, 1–14+98–101.
58. Jiao, P.; Guo, J.H.; Wang, X.K.; Liu, C.S.; Guo, X.W.; Huang, Y.R.; Liu, B. Characteristics and significance of petrological-mineralogical of lower Cambrian Niutitang formation shale gas reservoir in Northwest Hunan. *J. Cent. South Univ. Sci. Technol.* **2018**, *49*, 1447–1458.
59. Liu, Z.; Xu, L.; Wen, Y.; Zhang, Y.; Luo, F.; Duan, K.; Chen, W.; Zhou, X.; Wen, J. Accumulation Characteristics and Comprehensive Evaluation of Shale Gas in Cambrian Niutitang Formation, Hubei. *Eart. Scie.* **2022**, *47*, 1586. [[CrossRef](#)]
60. Wang, H. The influence of sample dissolution time in total organic carbon analysis results of the sedimentary rocks. *Petrochem. Ind. Appl.* **2015**, *34*, 87–92.
61. Liu, Z.; Algeo, T.J.; Guo, X.; Fan, J.; Du, X.; Lu, Y. Paleo-Environmental Cyclicity in the Early Silurian Yangtze Sea (South China): Tectonic or Glacio-Eustatic Control? *Palaeogeogr. Palaeoclimatol. Palaeoecol.* **2017**, *466*, 59–76. [[CrossRef](#)]
62. Qiu, X.S.; Hu, M.Y.; Hu, Z.G. Lithofacies palaeogeographic characteristics and reservoir-forming conditions of shale gas of lower Cambrian in middle Yangtze region. *J. Cent. South Univ. Sci. Technol.* **2014**, *45*, 3174–3185.
63. Lin, T.; Zhang, J.C.; Li, B.; Yang, S.Y.; He, W.; Tang, X.; Ma, L.R.; Pei, S.W. Shale gas accumulation conditions and gas-bearing properties of the lower Cambrian Niutitang Formation in Well Changye 1, northwestern Hunan. *Acta Pet. Sin.* **2014**, *35*, 839–846.
64. Liu, Z.B.; Wang, P.W.; Nie, H.K.; Li, P.; Li, Q.W. Enrichment conditions and favorable prospecting targets of Cambrian shale gas in Middle-Upper Yangtze. *J. Cent. South Univ. Sci. Technol.* **2022**, *53*, 3694–3707.
65. Luo, S.Y.; Chen, X.H.; Liu, A.; Li, H. Geochemical features and genesis of shale gas from the lower Cambrian Shuijingtuo Formation shale in Yichang block, Middle Yangtze region. *Oil Gas Geol.* **2019**, *40*, 999–1010.
66. Wu, S.; Hu, Z.G.; Qiu, X.S.; Li, S.L.; Li, H.D.; Liu, S.F. Mineral Composition and Its Significance of Organic Shale of the lower Cambrian Niutitang Formation in Tongshan Area, Eastern Hubei. *Sci. Technol. Eng.* **2020**, *20*, 11867–11874.
67. Liu, S.G.; Xie, G.L.; Yang, J.H. Formation Conditions of Shale Gas in Wangyinpu Formation of Jiurui Block in Northwest Jiangxi Province. *Spec. Oil Gas Reserv.* **2015**, *22*, 8–11+151.
68. Xia, X.J.; Hu, X.J.; Wang, C.Y. Shale Gas Accumulation Condition and Potential in lower Cambrian in Northwestern Jiangxi. *Spec. Oil Gas Reserv.* **2013**, *20*, 35–39+142.
69. Sing, K.S.W. Reporting Physisorption Data for Gas/Solid Systems with Special Reference to the Determination of Surface Area and Porosity (Recommendations 1984). *Pure Appl. Chem.* **1985**, *57*, 603–619. [[CrossRef](#)]
70. Thommes, M.; Kaneko, K.; Neimark, A.V.; Olivier, J.P.; Rodriguez-Reinoso, F.; Rouquerol, J.; Sing, K.S.W. Physisorption of Gases, with Special Reference to the Evaluation of Surface Area and Pore Size Distribution (IUPAC Technical Report). *Pure Appl. Chem.* **2015**, *87*, 1051–1069. [[CrossRef](#)]
71. Huang, Y.R.; Xiao, Z.H.; Jiao, P.; Qin, M.Y.; Yu, Y.; Wang, X.K.; Cao, T.T. Comparison of factors for shale gas accumulation in Niutitang formation wells in northwestern Hunan and its implications. *J. Cent. South Univ. Sci. Technol.* **2018**, *49*, 2240–2248.

72. Guo, C.L.; Yang, S.; Wang, A.D.; Zhang, S.L.; Qi, X. Pore Characteristics of Marine Shale in lower Cambrian Hetang Formation in Xiuwu Basin. *Xinjiang Pet. Geol.* **2020**, *41*, 550–556.
73. Chen, Y.Q.; Guo, E.P.; Qi, Y.D. A method for determining Langmuir's volume and Langmuir's pressure. *Fault-Block Oil Gas Field* **2015**, *22*, 67–69.
74. Loucks, R.G.; Reed, R.M.; Ruppel, S.C.; Hammes, U. Spectrum of Pore Types and Networks in Mudrocks and a Descriptive Classification for Matrix-Related Mudrock Pores. *AAPG Bull.* **2012**, *96*, 1071–1098. [[CrossRef](#)]
75. Ross, D.J.K.; Marc Bustin, R. The Importance of Shale Composition and Pore Structure upon Gas Storage Potential of Shale Gas Reservoirs. *Mar. Pet. Geol.* **2009**, *26*, 916–927. [[CrossRef](#)]
76. Behar, F.; Vandenbroucke, M. Chemical Modelling of Kerogens. *Org. Geochem.* **1987**, *11*, 15–24. [[CrossRef](#)]
77. Chalmers, G.R.L.; Bustin, R.M. Lower Cretaceous Gas Shales in Northeastern British Columbia, Part II: Evaluation of Regional Potential Gas Resources. *Bull. Can. Pet. Geol.* **2008**, *56*, 22–61. [[CrossRef](#)]
78. James, W. Schmoker (2) Determination of Organic-Matter Content of Appalachian Devonian Shales from Gamma-Ray Logs. *AAPG Bull.* **1981**, *65*, 1285–1298. [[CrossRef](#)]
79. Bowker, K.A. Barnett Shale Gas Production, Fort Worth Basin: Issues and Discussion. *AAPG Bull.* **2007**, *91*, 523–533. [[CrossRef](#)]
80. Milliken, K.L.; Curtis, M.E. Imaging Pores in Sedimentary Rocks: Foundation of Porosity Prediction. *Mar. Pet. Geol.* **2016**, *73*, 590–608. [[CrossRef](#)]
81. Soeder, D.J. The Successful Development of Gas and Oil Resources from Shales in North America. *J. Pet. Sci. Eng.* **2018**, *163*, 399–420. [[CrossRef](#)]
82. Nie, H.K.; Tang, X.; Bian, R.K. Controlling factors for shale gas accumulation and prediction of potential development area in shale gas reservoir of South China. *Acta Pet. Sin.* **2009**, *30*, 484–491.
83. Meyer, M.J.; Donovan, A.D.; Pope, M.C. Depositional Environment and Source Rock Quality of the Woodbine and Eagle Ford Groups, Southern East Texas (Brazos) Basin: An Integrated Geochemical, Sequence Stratigraphic, and Petrographic Approach. *AAPG Bull.* **2021**, *105*, 809–843. [[CrossRef](#)]
84. Wilson, M.J.; Wilson, L.; Shaldybin, M.V. The Importance of Illitic Minerals in Shale Instability and in Unconventional Hydrocarbon Reservoirs. *Geol. Soc. Lond. Spec. Publ.* **2017**, *454*, 253–269. [[CrossRef](#)]
85. Li, X.J.; Lv, Z.G.; Dong, D.Z.; Cheng, K.M. Geologic controls on accumulation of shale gas in North America. *Nat. Gas Ind.* **2009**, *29*, 27–32+135–136.
86. Fu, L.; Chen, Q.L.; Pan, J.Y.; Li, S.R. The reservoir characteristics of over-mature marine shale in the lower Yangtze plate: Taking the bottom lower Cambrian Hetang formation in the Xiuwu Basin as an instance. *Sci. Technol. Eng.* **2017**, *17*, 44–50.
87. Yao, H.S.; He, X.P.; Wang, K.M. Geochemical characteristics and significance of the shale of lower Cambrian Hetang Formation in the southern Anhui Province of Lower Yangtze area. *Mar. Geol. Front.* **2022**, *38*, 32–41. [[CrossRef](#)]
88. Zhu, D.; Lu, L.; Wei, J.Q.; Wang, F.; Gu, B.Y.; Pan, S.Y. Study of Vanadium in early Cambrian Black Shales—A Case Study of the Tongshan Mine, South China. *Resour. Environ. Eng.* **2018**, *32*, 473–480. [[CrossRef](#)]
89. Wu, Y.P.; Liu, C.L.; Gong, H.W.; Liu, Y.J.; Sarwar, A.R.; Yang, H.; Zeng, X.X. Geochemical characteristics and sedimentary tectonic setting of the lower Cambrian Niutitang Formation in western Hunan Province. *Geol. Explor.* **2021**, *57*, 1065–1076.
90. Dong, T.; He, S.; Chen, M.; Hou, Y.; Guo, X.; Wei, C.; Han, Y.; Yang, R. Quartz Types and Origins in the Paleozoic Wufeng-Longmaxi Formations, Eastern Sichuan Basin, China: Implications for Porosity Preservation in Shale Reservoirs. *Mar. Pet. Geol.* **2019**, *106*, 62–73. [[CrossRef](#)]
91. Xi, Z.; Tang, S.; Zhang, S.; Yi, Y.; Dang, F.; Ye, Y. Characterization of Quartz in the Wufeng Formation in Northwest Hunan Province, South China and Its Implications for Reservoir Quality. *J. Pet. Sci. Eng.* **2019**, *179*, 979–996. [[CrossRef](#)]
92. Zhang, K.; Li, Z.; Jiang, S.; Jiang, Z.; Wen, M.; Jia, C.; Song, Y.; Liu, W.; Huang, Y.; Xie, X.; et al. Comparative Analysis of the Siliceous Source and Organic Matter Enrichment Mechanism of the Upper Ordovician–Lower Silurian Shale in the Upper-Lower Yangtze Area. *Minerals* **2018**, *8*, 283. [[CrossRef](#)]
93. Korzhinsky, M.A.; Tkachenko, S.I.; Shmulovich, K.I.; Taran, Y.A.; Steinberg, G.S. Discovery of a Pure Rhenium Mineral at Kudriavyy Volcano. *Nature* **1994**, *369*, 51–52. [[CrossRef](#)]
94. Koschinsky, A.; Seifert, R.; Halbach, P.; Bau, M.; Brasse, S.; De Carvalho, L.M.; Fonseca, N.M. Geochemistry of Diffuse Low-Temperature Hydrothermal Fluids in the North Fiji Basin. *Geochim. Cosmochim. Acta* **2002**, *66*, 1409–1427. [[CrossRef](#)]
95. Mark, L.; Caplan, R. MARC BUSTIN Factors Governing Organic Matter Accumulation and Preservation in a Marine Petroleum Source Rock from the Upper Devonian to Lower Carboniferous Exshaw Formation, Alberta. *Bull. Can. Pet. Geol.* **1996**, *40*, 474–494.
96. Wan, T.F. *Chinese Geotectonics*; Geological Publishing House: Beijing, China, 2011.
97. Cai, Z.R.; Xia, B.; Huang, Q.T.; Wan, Z.F. Comparative Study of the Tectonic Setting on the Formation and Preservation of Paleozoic Shale Gas between the Upper Yangtze and the Lower Yangtze Platforms. *Nat. Gas Geosci.* **2015**, *26*, 1446–1454.
98. Teng, G.E.; Lu, L.F.; Yu, L.J.; Zhang, W.T.; Pan, A.Y.; Shen, B.J.; Wang, Y.; Yang, Y.F.; Gao, Z.W. Formation, preservation and connectivity control of organic pores in shale. *Pet. Explor. Dev.* **2021**, *48*, 687–699.
99. Hu, D.; Zhang, H.; Ni, K.; Yu, G. Preservation Conditions for Marine Shale Gas at the Southeastern Margin of the Sichuan Basin and Their Controlling Factors. *Nat. Gas Ind. B* **2014**, *1*, 178–184. [[CrossRef](#)]
100. Ingram, G.M.; Urai, J.L. Top-Seal Leakage through Faults and Fractures: The Role of Mudrock Properties. *Geol. Soc. Lond. Spec. Publ.* **1999**, *158*, 125–135. [[CrossRef](#)]
101. Wong, T.; Baud, P. The Brittle-Ductile Transition in Porous Rock: A Review. *J. Struct. Geol.* **2012**, *44*, 25–53. [[CrossRef](#)]

102. Fu, C.Q.; Zhu, Y.M.; Chen, S.B. Pore structure and fractal features of Hetang Formation shale in western Zhejiang. *J. China Univ. Min. Technol.* **2016**, *45*, 77–86. [[CrossRef](#)]
103. Cao, Q.G.; Cao, T.T.; Liu, G.X.; Song, Z.G.; Song, S.; Wang, S.B. Microscopic Pore Characteristics and Methane Sorption Capacity of the lower Cambrian Shales in Yangtze Platform. *Bull. Mineral. Petrol. Geochem.* **2016**, *35*, 1298–1309.
104. Zeng, W.T.; Ding, W.L.; Zhang, J.C.; Li, Y.X.; Wang, R.Y.; Jiu, K. Analyses of the characteristics and main controlling factors for the micro/nanopores in Niutitang shale from China's southeastern Chongqing and northern Guizhou region. *Earth Sci. Front.* **2019**, *26*, 220–235. [[CrossRef](#)]
105. Xiong, Q.; Peng, Y.; Tang, Y.J.; Chen, T.Y.; Mao, Y.H. Shale gas adsorption characteristics and influencing factors of Taiyuan Formation in Eastern Ordos Basin. *Geol. Surv. China* **2019**, *6*, 51–57. [[CrossRef](#)]
106. Wang, R.; Sang, S.; Zhu, D.; Liu, S.; Yu, K. Pore Characteristics and Controlling Factors of the lower Cambrian Hetang Formation Shale in Northeast Jiangxi, China. *Energy Explor. Exploit.* **2018**, *36*, 43–65. [[CrossRef](#)]
107. Guo, X.S. Rules of Two-Factor Enrichment for Marine Shale Gas in Southern China—Understanding from the Longmaxi Formation Shale Gas in Sichuan Basin and its surrounding area. *Acta Geol. Sin.* **2014**, *88*, 1209–1218. [[CrossRef](#)]
108. Cai, L.X.; Xiao, G.L.; Guo, X.W.; Wang, J.; Wu, Z.Q.; Li, B.G. Characteristics of Lower Silurian Hydrocarbon Source Rocks and their main controlling factors in the South Yellow Sea Basin based on Land-Ocean comparison in the Lower Yangtze region. *J. Jilin Univ. Earth Sci. Ed.* **2019**, *49*, 39–52. [[CrossRef](#)]
109. Zhai, G.Y.; Bao, S.J.; Wang, Y.F.; Chen, K.; Wang, S.J.; Zhou, Z.; Song, T.; Li, H.H. Reservoir Accumulation Model at the Edge of Palaeohigh and Significant Discovery of Shale Gas in Yichang Area, Hubei Province. *Acta Geosci. Sin.* **2017**, *38*, 441–447.
110. Shen, C.B.; Mei, L.F.; Liu, Z.Q.; Xu, S.H. Apatite and zircon fission track data, evidences for the mesozoic-cenozoic uplift of Huangling Dome, Central China. *Miner. Pet.* **2009**, *29*, 54–60. [[CrossRef](#)]
111. Zhai, G.Y.; Wang, Y.F.; Liu, G.H.; Lu, Y.C.; He, S.; Zhou, Z.; Li, J.; Zhang, Y.X. Accumulation model of the Sinian-Cambrian shale gas in western Hubei Province, China. *J. Geomech.* **2020**, *26*, 696–713.
112. Shkolin, A.V.; Fomkin, A.A. Deformation of AUK Microporous Carbon Adsorbent Induced by Methane Adsorption. *Colloid. J.* **2009**, *71*, 119–124. [[CrossRef](#)]
113. Zhang, J.C.; Li, Z.; Wang, D.S.; Xu, L.F.; Li, Z.M.; Niu, J.L.; Chen, L.; Sun, Y.H.; Li, Q.C.; Yang, Z.K.; et al. Shale gas accumulation patterns in China. *Nat. Gas Ind.* **2022**, *42*, 78–95. [[CrossRef](#)]
114. Fernando De Ros, L. Heterogeneous Generation and Evolution of Diagenetic Quartzarenites in the Silurian-Devonian Furnas Formation of the Paraná Basin, Southern Brazil. *Sediment. Geol.* **1998**, *116*, 99–128. [[CrossRef](#)]
115. Einsele, G.; Gieskes, J.M.; Curray, J.; Moore, D.M.; Aguayo, E.; Aubry, M.-P.; Fornari, D.; Guerrero, J.; Kastner, M.; Kelts, K.; et al. Intrusion of Basaltic Sills into Highly Porous Sediments, and Resulting Hydrothermal Activity. *Nature* **1980**, *283*, 441–445. [[CrossRef](#)]
116. Othman, R.; Aroui, K.R.; Ward, C.R.; McKirdy, D.M. Oil Generation by Igneous Intrusions in the Northern Gunnedah Basin, Australia. *Org. Geochem.* **2001**, *32*, 1219–1232. [[CrossRef](#)]
117. He, Z.; Nie, H.; Li, S.; Luo, J.; Wang, H.; Zhang, G. Differential Enrichment of Shale Gas in Upper Ordovician and Lower Silurian Controlled by the Plate Tectonics of the Middle-Upper Yangtze, South China. *Mar. Pet. Geol.* **2020**, *118*, 104357. [[CrossRef](#)]
118. Meng, F.Y.; Chen, K.; Bao, S.J.; Li, H.H.; Zhang, C.; Wang, J.Z. Gas-bearing property and main controlling factors of lower Cambrian shale in complex tectonic area of northwestern Hunan province: A case of well Ciye 1. *Lithol. Reserv.* **2018**, *30*, 29–39.
119. Zhang, F.Y. Lower Yangtze Region lower Cambrian Series Source Rock Geochemical Features Analysis. *Coal Geol. China* **2018**, *30*, 36–42. [[CrossRef](#)]
120. Liu, Z.P.; Xu, W.; Wang, J.T.; Wang, Y.G.; Zhou, C.T. Analysis of geological conditions of gas formation in the Low Yangtze Area in early Cambrian. *Geol. Anhui* **2015**, *25*, 111–114+118.
121. Shao, W.; Huang, Z.Q.; Li, J.Q.; Zhou, D.R. Shale gas reservoir-forming conditions and exploration prospecting in the Cambrian Hetang Formation of southwestern Zhejiang and northeastern Jiangxi Province. *Geol. China* **2022**, *49*, 1262–1274.

Disclaimer/Publisher's Note: The statements, opinions and data contained in all publications are solely those of the individual author(s) and contributor(s) and not of MDPI and/or the editor(s). MDPI and/or the editor(s) disclaim responsibility for any injury to people or property resulting from any ideas, methods, instructions or products referred to in the content.